www.sciencemag.org/content/356/6333/44/suppl/DC1

Supplementary Material for

Reovirus infection triggers inflammatory responses to dietary antigens and development of celiac disease

Romain Bouziat, Reinhard Hinterleitner, Judy J. Brown, Jennifer E. Stencel-Baerenwald, Mine Ikizler, Toufic Mayassi, Marlies Meisel, Sangman M. Kim, Valentina Discepolo, Andrea J. Pruijssers, Jordan D. Ernest, Jason A. Iskarpatyoti, Léa M. M. Costes, Ian Lawrence, Brad A. Palanski, Mukund Varma, Matthew A. Zurenski, Solomiia Khomandiak, Nicole McAllister, Pavithra Aravamudhan, Karl W. Boehme, Fengling Hu, Janneke N. Samsom, Hans-Christian Reinecker, Sonia S. Kupfer, Stefano Guandalini, Carol E. Semrad, Valérie Abadie, Chaitan Khosla, Luis B. Barreiro, Ramnik J. Xavier, Aylwin Ng, Terence S. Dermody,* Bana Jabri*

*Corresponding author. Email: bjabri@bsd.uchicago.edu (B.J.); terence.dermody@chp.edu (T.S.D.)

Published 7 April 2017, *Science* **356**, 44 (2017)
DOI: 10.1126/science.aah5298

This PDF file includes:

Materials and Methods

Mice

All knockout and transgenic mice used in these studies are on a C57BL/6 background. C57BL/6 (WT), IFNAR$^{-/-}$ (B6.129S2-*Ifnar1*^{tm1Agt}/Mmjax) and IRF1$^{-/-}$ (B6.129S2-*Irf1*^{tm1Mak}/J) were purchased from Jackson Laboratories. RAG$^{-/-}$ OT-II$^{+/-}$ CD45.1$^{+/+}$ mice were provided by Dr. Peter Savage and bred and housed in our animal facility. HLA-DQ8 transgenic (DQ8tg) mice were previously described (*47*) and maintained on a gluten-free diet (AIN76A, Envigo). TG2$^{-/-}$ mice were previously described (*48*). For all experiments, mice were analyzed at 6-8 weeks of age. C57BL/6 mice were maintained in an SPF environment at the University of Chicago and Vanderbilt University. IFNAR$^{-/-}$, IRF1$^{-/-}$, RAG$^{-/-}$ OT-II$^{+/-}$ CD45.1$^{+/+}$ and DQ8tg mice were housed exclusively at the University of Chicago. Experiments comparing WT and knock out mice were performed either using littermate controls or mice that were co-housed for 15 to 21 days. Animal husbandry and experimental procedures were performed in accordance with Public Health Service policy and approved by the University of Chicago and Vanderbilt University School of Medicine Institutional Animal Care and Use Committees.

Cells and viruses

Spinner-adapted murine L929 (L) cells were grown in either suspension or monolayer cultures in Joklik's modified Eagle's minimal essential medium (SMEM; Lonza) supplemented to contain 5% fetal bovine serum (FBS; Gibco), 2 mM L-glutamine, 100 U/ml penicillin, 100 μg/ml streptomycin (Gibco), and 25 ng/ml amphotericin B (Sigma). BHK-T7 cells were grown in Dulbecco's modified Eagle's minimal essential medium (DMEM; Gibco) supplemented to contain 5% FBS, 2 mM L-glutamine, 1 mg/ml geneticin (Gibco), and nonessential amino acids (Sigma). Caco-2 cells were grown in DMEM supplemented to contain 10% FBS, 100 U/ml penicillin, 100 μg/ml streptomycin, 1 mM sodium pyruvate (Gibco), nonessential amino acids, and 12.5 ng/ml amphotericin B. Caco-2 cells were plated at a density of 10^5 cells/well in 24-well plates (Costar). Rhesus monkey kidney (MA104) cells were provided by Dr. John Patton and grown in DMEM supplemented to contain 5% FBS, 2 mM L-glutamine, nonessential amino acids, and 1 mg/ml geneticin as previously described (*49*). Mouse embryonic fibroblasts (MEFs) from C57BL/6 mice were grown in DMEM supplemented to contain 10% FBS, 2 mM L-glutamine, 100 U/ml penicillin, 100 μg/ml streptomycin, and nonessential amino acids.

Recombinant reoviruses were generated using plasmid-based reverse genetics (*50*). Recombinant strain (rs) type 1 Lang (T1L) is a stock generated by plasmid-based rescue from cloned T1L cDNAs (*51*). The engineered reassortant virus strain, T3D-RV, was recovered following transfection of BHK-T7 cells with plasmid constructs encoding the S1 and L2 gene segments from strain T1L and the remaining eight gene segments from strain type 3 Dearing (T3D). After 3 to 5 days of incubation, cells were frozen and thawed three times, and virus was isolated by plaque purification using monolayers of L cells (*52*). Purified reovirus virions were generated from second- or third-passage L cell lysate stocks (*53*). Viral particles were extracted from infected cell lysates using Vertrel XF (DuPont), layered onto 1.2- to 1.4- g/cm^3 CsCl gradients, and centrifuged at 62,000 x

g for 16 hours. Bands corresponding to virions (1.36 g/cm^3) were collected and dialyzed in virion storage buffer (150 mM NaCl, 15 mM $MgCl_2$, and 10 mM Tris-HCl [pH 7.4]) (*54*). Viral titer was determined by plaque assay using L cells (*52*). Purified viral particles were electrophoresed on SDS-polyacrylamide gel. The gel was stained with ethidium bromide to visualize viral gene segments.

Infection of mice

Mice were inoculated perorally with purified reovirus diluted in phosphate-buffered saline (PBS) using a 22-gauge round-tipped needle (Cadence Science) (*55*). Titers of virus in the inocula were determined to confirm the number of infectious particles in the administered dose. For analysis of viral titer, mice were euthanized at various intervals post-inoculation, organs were harvested into 1 ml of PBS and stored at -80 °C prior to assay. Samples were thawed (37 °C), bead beaten for 8 minutes, frozen (-80 °C), and bead beaten again for 5 minutes prior to quantitation by plaque assay. Viral titers in organ homogenates were determined as the number of plaque forming units (PFU) per ml of tissue or cell-culture homogenate (*52*). All of our initial studies, with the exception of the genomic studies that analyzed different tissue compartments, were performed 6 days after inoculation with 10^{10} PFU of virus. Analysis of dendritic cells (DC) in WT and in IFNAR$^{-/-}$ mice upon reovirus infections was performed at 48h, and required the adjustment of the amount of virus used for infection to 10^8 PFU. Indeed, at that time point and with a dose of 10^{10} PFU of virus, the titers of reovirus in the mesenteric lymph nodes (mLN) are high (10^{7-8} PFU), especially in IFNAR$^{-/-}$ mice, and the immune system is hyperactivated, hampering the ability to detect quantitative differences between viruses and genotypes. The same dose of 10^8 PFU of virus was used when T cell responses to dietary antigens were analyzed in IFNAR$^{-/-}$ and IRF1$^{-/-}$ mice at 48 hours.

Antibodies and flow cytometry

The following fluorophore conjugated antibodies were purchased from eBioscience: T-bet (4B10), Foxp3 (FJK-16s), MHCII (M5/114.15.2), CD11b (M1/70), IL-12p40 (C17.8), CD62L (MEL-14), CD25 (PC61.5), Rat IgG1, Rat IgG2a, Rat IgG2b and Mouse IgG1. The following antibodies were purchased from BD Biosciences: IFNγ (XMG1.2), CD103 (M290), CD45 (30-F11), and Fc Block™ (2.4G2). The following antibodies were purchased from Biolegend: CD4 (GK1.5), TCRb (H57-597), CD45.1 (A20), CD11c (N418), CD8a (53-6.7), CD86 (GL-1), CD44 (IM7), and F4/80 (BM8). Immunoglobulin G (IgG) fractions of rabbit antisera raised against reovirus strains (T1L) and (T3D) (*56*) were purified by protein A sepharose chromatography (*57*). Aqua LIVE/DEAD® Fixable Aqua Dead Cell Stain Kit was purchased from Life Technologies. Cells were permeabilized with the Foxp3 fixation/permeabilization kit for transcription factor (eBioscience) or Cytofix/Cytoperm (BD Biosciences) for cytokine staining. Flow cytometry was performed with a 9-color BD FACSCanto (BD Biosciences) and data were analyzed using FlowJo software (Treestar). Sorting experiments were performed with an Aria Fusion (BD Biosciences).

Assays of reovirus replication, infectivity and type-1 interferon response

Caco-2 cells were adsorbed with reovirus at a multiplicity of infection (MOI) of 0.1, 1, or 10 PFU/cell, washed with PBS, and incubated at 37 ºC for various intervals. Cells were frozen and thawed twice prior to determination of viral titer by plaque assay using L cells

(*52*) or lysed for analysis of type-1 interferon inducible genes by RT-PCR. Mouse embryonic fibroblasts (MEFs) were adsorbed with reovirus at a MOI of 500 PFU/cell, washed with PBS, and incubated at 37 ºC for 16 hours. Supernatants were analyzed for IFNβ by ELISA (PBL Interferon Source).

Histology and immunohistochemistry

Mice were inoculated perorally with purified reovirus diluted in PBS. At 1 and 8 days post-inoculation (dpi), mice were euthanized, and intestines of infected mice were resected. The proximal half was prepared for viral titer determination by plaque assay, and the distal half was flushed with 10% formalin and Swiss-rolled. Samples were submerged in 10% formalin at room temperature for 24 or 48 hours and embedded in paraffin. Consecutive 6-µm sections were stained with hematoxylin and eosin (H&E) for evaluation of histopathologic changes or processed for immunohistochemical detection of reovirus antigen. Images were captured at 20x magnification at a resolution of 0.5 µm/pixel using a high-throughput Leica SCN400 slide scanner automated digital imaging system.

Isolation of Peyer's patches, intestinal epithelium and lamina propria

Peyer's patches (PP) were removed, treated with collagenase VIII (Sigma) and processed by mechanical disruption through a 70-µm cell strainer. The intestinal epithelium was isolated as previously described using RPMI media containing 2 mM EDTA (Corning), 1% dialyzed FBS, and 1.5 mM $MgCl_2$. The lamina propria (Lp) was isolated as previously described using RPMI media containing 20% FBS and collagenase VIII (Sigma) (*47*).

In vivo T cell conversion assays

To assess T cell conversion *in vivo*, $CD4^+$ T cells were purified from the spleen and lymph nodes of $RAG^{-/-}$ $OT\text{-}II^{+/-}$ $CD45.1^{+/+}$ mice using the $CD4^+$ T cell isolation Kit (Miltenyi) or sorted on a FACS Aria Fusion (BD Biosciences). $4x10^5$ to $7.5x10^5$ cells were transferred retro-orbitally into congenic naïve C57BL/6 mice. Mice received ovalbumin (OVA) (grade V, Sigma) dissolved in the drinking water (1.5%) for 2 or 6 days, as indicated or were fed an OVA-containing diet (Harlan Envigo TD 130362 10mg/kg) for 6 days. One day after transfer, mice were infected perorally with equal PFU of T1L or T3D-RV as indicated or injected intraperitoneally (i.p.) every other day with 50 ug of polyinosinic:polycytidylic acid (poly(I:C)) (Invivogen) or 1000 IU of mIFNβ (PBL Interferon Source). Mice were euthanized and intranuclear levels of Foxp3, T-bet, or cytokine IFNγ were evaluated by flow cytometry in transferred $CD45.1^+$ and recipient T cells from mLN incubated in the presence of 50 ng/ml phorbol 12-myristate 13-acetate (PMA), 500 ng/ml ionomycin (Sigma) and 1.3 µl/ml Golgi Stop (BD Biosciences) for 2 hours at 37 ºC, 5% CO_2. For IL-12 staining, cells were incubated in RPMI (Corning) for 6 hours at 37 ºC, 5% CO_2 in the presence of 1 µl/ml Golgi Plug (BD Biosciences).

In vitro T cell conversion assays

mLN DC subsets ($CD103^+$ $CD11b^-$ $CD8\alpha^+$, $CD103^+$ $CD11b^-$ $CD8\alpha^-$, $CD103^+$ $CD11b^+$, $CD103^-$ $CD11b^+$) were FACS sorted (Aria Fusion BD Biosciences) 2 days after inoculation of WT or $IRF1^{-/-}$ mice with T1L or PBS (sham). DC subsets were then mixed

back at a WT ratio and $5x10^3$ DC / mix were co-cultured for 5 days with $2.5x10^4$ FACS sorted naïve $CD4^+$ T cells (Aria Fusion BD Biosciences) from the spleen and lymph nodes of $RAG^{-/-}$ $OT\text{-}II^{+/-}$ $CD45.1^{+/+}$ mice in presence of 100 µg/ml of OVA (Sigma) with or without 1µg/ml of anti-mouse IL-12p40 neutralizing antibody (BD Pharmingen).

Analysis of cytokine production

IFNγ and IL-12p40 cytokine levels in culture supernatants were determined with BioPlex multianalyte technology (Biorad).

Oral tolerance assay

Mice were inoculated perorally with purified reovirus diluted in PBS or with PBS alone. 100 µg OVA (grade V, Sigma) feeding occurred every other day for 8 days. At day 10 mice were immunized with complete Freund's adjuvant (CFA)-OVA (emulsion of 50 µl CFA (Sigma) and 50 µl PBS containing 100 µg OVA) subcutaneously at the back left and right flank. Draining lymph nodes (dLN) were harvested on day 18 and cells were restimulated for 48 hours with OVA. Supernatants were analyzed for IFNγ by ELISA (BD Biosciences). Alternatively, when indicated, mice were fed an OVA-containing diet (10 mg/kcal, Envigo) for 8 days. At day 10, mice were immunized subcutaneously between the shoulder blades with an emulsion of 100 µl CFA and 100 µl PBS containing 300 µg OVA under isofluorane gas anesthesia. At day 18, mouse sera were obtained by submandibular bleeding for anti-OVA IgG2c ELISA quantification.

Preparation of chymotrypsin-digested gliadin (CT-gliadin)

Gliadin (Sigma) was dissolved in 2 M NH_4HCO_3 2 M urea buffer pH 8.0, by vortexing and digested using a-chymotrypsin (Sigma) for 24 hours on a roller mixer at room temperature. The reaction was stopped by incubation at 98 ºC for 10 minutes. Digested gliadin was filtered through a 0.45 µm membrane (Millipore) and dialyzed against sterile PBS using snakeskin dialysis tubing with a molecular weight cut-off of 3.5 kDa (Thermo Scientific). Concentration of CT-gliadin was determined using a BCA assay (Pierce).

Oral antigen uptake by dendritic cells

OVA or CT-gliadin was labeled with Alexa Fluor-647 succinimidyl ester according to the manufacturer's protocol (Molecular Probes). Mice received 3.2 mg OVA-Alexa Fluor-647 or Gliadin-Alexa Fluor-647 by intragastric administration, respectively. Control mice received similar amounts of unlabeled OVA or CT-gliadin (*58*). Mice were euthanized 18 hours post-feeding and DCs in mLN were analyzed by flow cytometry.

CFA immunization and subcutaneous ear challenge

DQ8tg mice received 50 mg CT-gliadin orally for 2 days. At the start of feeding mice were inoculated perorally with purified T1L. Two days after CT-gliadin administration, CFA-CT-gliadin was administered subcutaneously between the shoulder blades as an emulsion of 100 µl CFA and 100 µl PBS containing 300 µg CT-gliadin under isofluorane gas anesthesia. Ear challenges were performed 14 and 24 days after immunization. A volume of 20 µl of 100 µg CT-gliadin / PBS was injected under isofluorane gas anesthesia. Ear thickness was measured on days 1, 2, and 3 after each CT-gliadin challenge using a digital precision caliper (Fisher Scientific). Swelling was determined by subtracting pre-challenge from post-challenge ear thickness.

Anti-OVA and anti-gliadin IgG2c ELISA

High-binding ELISA 96-well plates (Corning) were coated with 50 µl of 10 µg/ml OVA in PBS or 50 µl of 100 µg/ml CT-gliadin in 100 mM Na_2HPO_4 overnight at 4 °C. Plates were washed three times with PBS 0.05% Tween 20 and blocked with 200 µl of PBS 10% FBS (Anti-OVA ELISA) or 200 µl of 2% BSA in PBS 0.05% Tween 20 (Anti-gliadin ELISA) for 2 hours at room temperature. Unlabeled IgG2c (SouthernBiotech) was used as positive control. Serum was assessed in duplicate and at two dilutions, typically 1/1000 and 1/5000. Sera were incubated overnight at 4 °C and plates were washed three times with PBS 0.05% Tween 20. Anti-mouse IgG2c-horseradish peroxidase (HRP) (SouthernBiotech) in blocking buffer (50 µl at 1/500 dilution) was added to plates and incubated for 1 hour at room temperature. Plates were washed five times with PBS containing 0.05% Tween 20. HRP substrate TMB (50 µl) was added and the reaction stopped by the addition of 50 µl 2 N H_2SO_4. Absorbance was read at 450 nm. Levels of anti-OVA IgG2c or anti-gliadin IgG2c were expressed in OD values.

Visualization and quantification of TG2 activity

DQ8tg or $TG2^{-/-}$ mice were inoculated perorally with purified T1L reovirus diluted in PBS or with PBS alone and *in vivo* TG2 enzymatic activity was assessed 18 hours post infection, essentially as previously described (*59*). Six and three hours prior to euthanasia, mice were injected i.p. (100 mg/kg) with 5-(biotinamido)-pentylamine (5BP), a substrate for TG2 transamidation activity, which was synthesized following a published protocol (*59*). Small intestinal pieces were collected and frozen in optimum cutting temperature (OCT) compound (Tissue-Tek). Frozen sections of 5 µm thickness were cut, fixed in 1% paraformaldehyde, and TG2 protein was visualized by staining with a rabbit polyclonal anti-TG2 antibody (custom produced by Pacific Immunology), followed by AF647-conjugated goat anti-rabbit IgG (LifeTechnologies). TG2 enzymatic activity was measured using 5BP crosslinking, and was visualized by costaining with AF555-conjugated streptavidin (LifeTechnologies). Images were acquired at 10x magnification using a Leica SP8 Laser Scanning Confocal microscope. TG2 activity was quantified by systematically taking two sections of proximal small intestine from each mouse, quantifying the 5BP signal / TG2 protein signal on a per villi basis. The mean 5BP signal / TG2 signal is shown for each mouse that was assessed.

Human tissue and serum samples

Serum and duodenal biopsies were collected from consented controls or patients with celiac disease. Diagnosis of celiac disease was based on detection of anti-transglutaminase antibodies, villous atrophy, and clinical response to gluten-free diet. Gluten-free subjects had been under strict gluten-free diet (GFD) for at least 1 year and had become negative for anti-transglutaminase antibodies and recovered a normal or subnormal villous architecture (*60*). Control subjects with normal small intestinal histology, no family history of CD and no TG2 antibodies, underwent gastrointestinal endoscopy for a diagnostic work-up (e.g., for evaluation of anemia, abdominal discomfort, intestinal disorders of non-celiac origin, or failure to thrive) (*61*).

Control patients: Age range 1-77 (average 24.06); 56.94% females, 43.06% males.
Active patients: Age range 2-69 (average 26.21); 66.21% females, 33.79% males.

GFD patients: Age range 2-79 (average 35.13); 70.5% females, 29.5% males.
These studies were approved by the University of Chicago Institutional Review Board.

Quantification of virus-specific antibody responses

Reovirus-specific antibody responses were determined using a 60% plaque-reduction neutralization assay (PRNT 60). Serum samples were heat-inactivated at 56 ºC for 30 minutes, serially diluted four-fold beginning with a dilution of 1:20, and incubated with an equal volume of a virus stock containing 100 PFU of T1L for 1 hour. The serum-virus mixtures were inoculated in duplicate onto confluent L cell monolayers in 12-well tissue culture plates (Costar), incubated at room temperature for 1 hour, and overlayed with a 1:1 mixture of 1% agar (BD Biosciences) and 2x199 medium (Caisson labs) supplemented to contain 5% FBS, 4 mM L-glutamine, 200 U/ml penicillin, 200 µg/ml streptomycin (Gibco), and 50 ng/ml amphotericin B (Sigma). Cells were stained with neutral red on day 7, and plaques were enumerated (*52*). Serum reciprocal geometric mean titers capable of reducing plaque counts by 60% were calculated using regression analysis.

Rotavirus-specific antibody responses were determined using PRNT 60 assay with simian rotavirus strain SA11 and MA104 cells both provided by Dr. John Patton. Serum samples were heat-inactivated at 56 ºC for 30 minutes, serially diluted four-fold beginning with a dilution of 1:20, and incubated with an equal volume of a previously trypsin-activated rotavirus stock containing 100 PFU. After incubation for 1 hour, the serum-virus mixtures were inoculated in duplicate onto confluent MA104 cell monolayers in 12-well tissue-culture plates. On day 3, cells were fixed with neutral-buffered formalin at room temperature for 1 hour, stained with crystal violet, and plaques were enumerated (*49*). Serum reciprocal geometric mean titers capable of reducing plaque counts by 60% were calculated using regression analysis.

Qualitative detection of Herpes Simplex Virus Type 1 (HSV-1) IgG antibodies were determined in serum samples using the Zeus Scientific ELISA HSV-1 IgG Test System (Alere) according to manufacturers' instructions. These studies were approved by the Vanderbilt University School of Medicine Institutional Review Board.

RT-PCR

RNA was prepared using the RNeasy Mini Kit (Qiagen) or High Pure RNA isolation kit (Roche). cDNA synthesis was performed using GoScript (Promega) or Superscript III First-Strand Synthesis System (Invitrogen) according to the manufacturer's instructions. Expression analysis was performed in duplicate via real-time PCR on a Roche LightCycler 480 using SYBR Green (Clontech) or an Applied Biosystems 7500 Real-Time PCR system (Life Technologies) with a Power SYBR Green Master Mix (Thermo Fisher Scientific). Expression levels were quantified and normalized to *Gapdh* expression using the following primer pairs:

Species	Gene	Forward Primer	Reverse Primer
Murine	*Gapdh*	AGGTCGGTGTGAACGGATTTG	TGTAGACCATGTAGTTGAGGTCA
Murine	*Irf1*	CAGAGGAAAGAGAGAAAGTCC	CACACGGTGACAGTGCTGG
Murine	*Isg15*	GGTGTCCGTGACTAACTCCAT	TGGAAAGGGTAAGACCGTCCT
Murine	*Mx1*	GACCATAGGGGTCTTGACCAA	AGACTTGCTCTTTCTGAAAAGCC

Murine	*Il12b*	ACAGCACCAGCTTCTTCATCAG	TCTTCAAAGGCTTCATCTGCAA
Murine	*Il27*	CTCTGCTTCCTCGCTACCAC	GGGGCAGCTTCTTTTCTTCT
Human	*GAPDH*	ATGGGGAAGGTGAAGGTCG	GGGGTCATTGATGGCAACAATA
Human	*MX1*	CAGCACCTGATGGCCTATCA	TGGAGCATGAAGAACTGGATGA
Human	*ISG15*	GAGAGGCAGCGAACTCATCT	CTTCAGCTCTGACACCGACA
Human	*IRF1*	GCAGCTACACAGTTCCAGG	GTCCTCAGGTAATTTCCCTTCCT

Expression analysis for murine *Ifna2/Ifna11* was performed with TaqMan gene-expression assays and normalized to *Gapdh* (Applied Biosystems).

Transcriptomics (microarray and RNA-sequencing analysis)

Gene expression was profiled using Illumina Mouse Expression BeadChip WG-6 according to manufacturer's instructions. Array data was background corrected using BeadStudio and quantile normalized. A linear model was applied and implemented in the R programming language, utilizing functions from linear models for microarray data. For each probe, a moderated t-statistic (with standard errors moderated across genes) was computed using a Bayesian model to assess differential expression (*62*). The associated p-values were adjusted to control the false discovery rate in multiple testing, using the Benjamini and Hochberg's (BH) method (BH-adjusted $p<0.05$) (*63*). Multiple dimensional scaling (MDS) was applied to visualize profiles assembled from genes that were identified as differentially expressed in each state across the tissue types examined. MDS facilitates the representation of distances between pairs of samples in lower dimensional space and samples are assigned 'coordinates' in each dimension. By applying Prim's algorithm implemented as priority-first search for graphs (*64*), a minimum spanning tree (for dissimilarities) that connected all vertices or nodes (denoting the profile vector for each sample) was found by minimizing the total weighting for its edges.

For RNA-seq, RNA libraries were prepared using the TruSeq® Stranded Total RNA with Ribo-Zero™ Gold kit (Illumina) and sequenced using 50-base pair single-end reading on a HiSeq 2500 instrument (Illumina). Reads were mapped to the mouse genome (mm10) using Tophat2 (*65*). To improve mapping, a GTF-file containing exon boundaries of all known RefSeq genes was supplied to Tophat. Quality control was performed using the RSEM-based quantification approach (*66*). HTSeq was used to count features from the alignment files. The count data was normalized by the trimmed mean of M-values normalization (TMM) method, followed by variance estimation and applying generalized linear models (GLMs) in the R language, implementing empirical analysis of digital gene expression (*67*) to identify differentially expressed genes. Factorial designs were incorporated into the analysis by fitting these linear models with the coefficient for each of the factor combinations and then simultaneously extracting contrasts (*67*) for the respective 'differential-of-differential' analysis in the two experimental dimensions (virus infection and genotype status: WT and $IFNAR^{-/-}$).

Enrichment analysis of pathway / biological processes and semantic similarity clustering

Pathway and biological process enrichment analysis were performed as previously described (*68-70*). Briefly, data were interrogated from KEGG pathways and gene ontology biological processes. Each module or category was assessed for statistical

enrichment or over-representation among differentially expressed genes relative to their representation in the global set of genes in the genome. Nominal p- and Benjamini-Hochberg-adjusted p-values were computed using the hypergeometric test implemented in the R programming language. Following enrichment analysis, pathways and biological processes derived from gene ontology and identified as over-represented were further subjected to gene semantic similarity analysis to establish similarity or 'relatedness' between pathway/process categories, by applying node-based measures of information content (IC), i.e. how informative or specific each pathway/process category, *c* is. IC is defined as the negative log likelihood for the occurrence of *c* in the pathway/process knowledgebase or in the most informative common ancestor in the ontology hierarchy, c_{MICA} (*71*). We utilized the relevance similarity measure (*72*) , sim_{Rel} :

$$sim_{Rel}(c_1, c_2) = \frac{2IC(c_{MICA})}{IC(c_1) + IC(c_2)} \times (1 - p(c_A))$$

A semantic similarity map was generated by performing hierarchical clustering using the Minkowski distance metric on the resulting symmetric matrix of sim_{Rel} values for each pairwise comparison between pathway/process categories.

Statistical Analysis

Data were first analyzed for normal distribution using D'Agostino and Pearson omnibus normality tests. Normally distributed data was analyzed using unpaired two-tailed Student's *t*-test for single comparisons, and one-way ANOVA for multiple comparisons. ANOVA analysis was followed by a Tukey's post-hoc test. Not normally distributed data was analyzed using unpaired two-tailed Mann-Whitney *U*-test for single comparisons. The statistical test used and *P* values are indicated in each figure legend. P values of < 0.05 were considered to be statistically significant. *P < 0.05, **P < 0.01, ***P < 0.001 and ****P < 0.0001. ns = non significant.

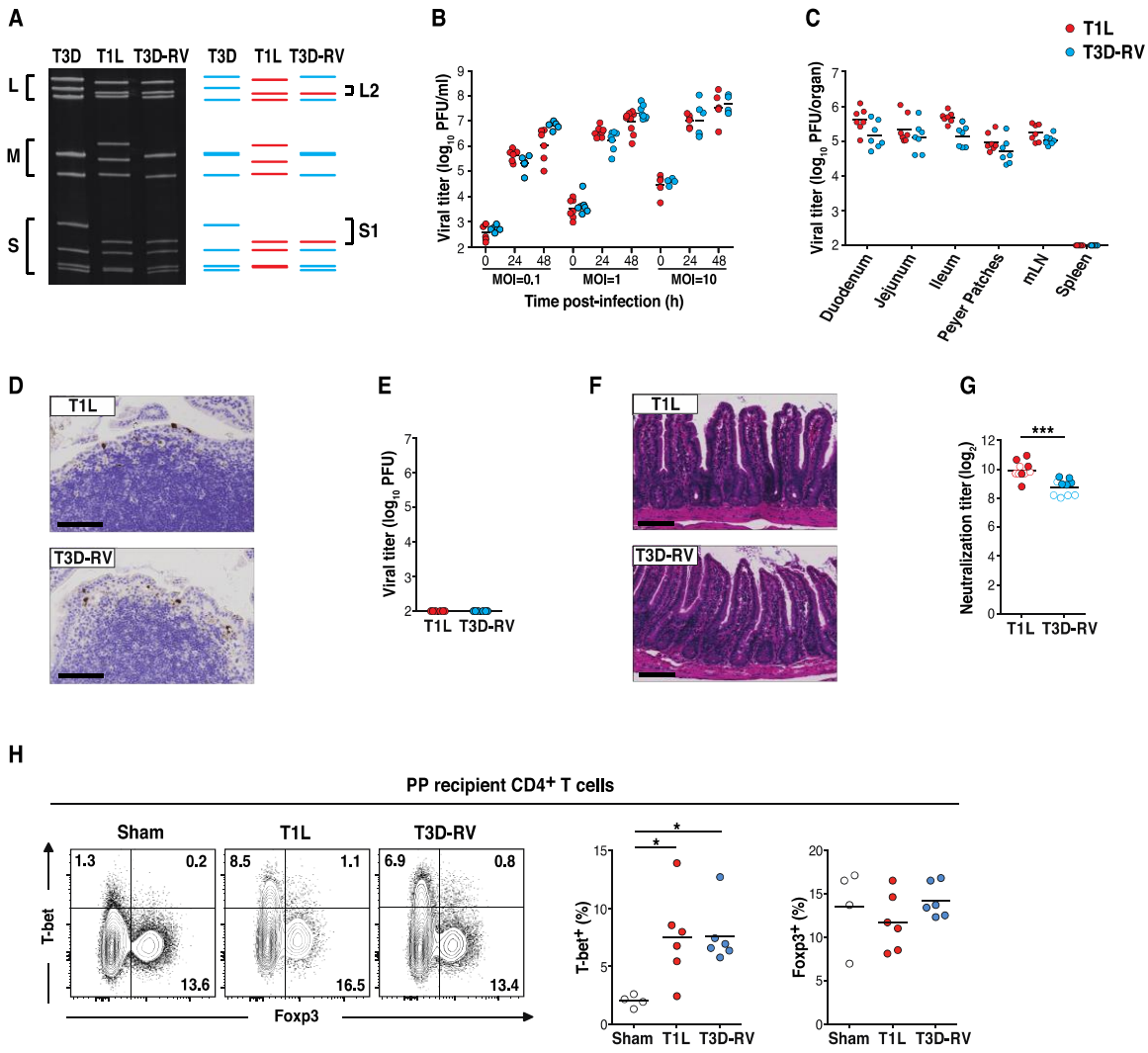

Fig. S1.

Experimental model of viral infection using genetically engineered reoviruses (**A**) Electropherotypes and schematic of T1L, T3D, and T3D-RV gene segments. Purified viral particles were electrophoresed in an SDS-polyacrylamide gel, which was stained with ethidium bromide to visualize viral gene segments. Size classes of gene segments, large (L), medium (M), and small (S) are indicated. (**B**) Titers of T1L (red circles) and T3D-RV (blue circles) in Caco-2 cells were determined at the indicated times and MOIs by plaque assay. (**C** to **H**) WT mice were inoculated perorally with 10^{10} plaque forming units (PFU) of T1L or T3D-RV. (C) Titers of T1L (n = 7) and T3D-RV (n = 7) in the indicated small intestinal compartments, Peyer's patches (PP), mesenteric lymph nodes (mLN) and spleen were determined at 24 hours post-inoculation (hpi) by plaque assay. The small intestine was resected from the pylorus to the cecum and sectioned into three equal parts comprising the duodenum, jejunum and ileum. Viral loads following T1L and T3D-RV infections were comparable in all tissues assayed with the exception of the ileum, where the titer produced by T1L was ~ 3-fold greater than that produced by T3D-RV. However, this difference was not statistically significant (One-way ANOVA, P >

0.05). (D) At 24 hpi, small intestines of infected mice were resected and processed for histology. Sections were stained with polyclonal reovirus antiserum (brown). Representative sections of PP are shown (scale bar: 100 μm). (E) At 6 days post-inoculation (dpi), the ileum was resected, and titers of T1L and T3D-RV were determined by plaque assay (n = 6 mice per virus strain). (F) At 8 dpi, small intestines of infected mice were resected and processed for histology. Sections were stained with hematoxylin and eosin. Representative sections of ileum are shown (scale bar: 100 μm). (G) At 18 (open circles) or 21 (filled circles) dpi, sera were collected, heat-inactivated, and used for a plaque-reduction neutralization assay (n = 10 mice per virus strain). (H) The intracellular expression of Foxp3 and T-bet in PP $CD4^+$ T cells at 6 dpi was evaluated by flow cytometry. Representative dot plots and percentages of Foxp3- and T-bet-expressing $CD4^+$ T cells are shown. (B) Data represent two independent experiments performed in triplicate. (C, E, G, and H) Graphs depict two independent experiments. (B, C and H) *P < 0.05 (One-way ANOVA / Tukey's multiple comparison). (E and G) ***P < 0.001 (unpaired t-test).


Early (6h) impact by T1L and T3D-RV
Epithelium
Lp
PP
mLN
Late (48h) impact by T1L and T3D-RV
Late (48h) impact by T1L and T3D-RV (cont'd)
Log2FC or Log2Expression (Z-transformed)

Fig. S2.

Temporal and spatial gene expression in response to reovirus infection. Heatmap shows the subset of the 2307 gene features used for generation of the spanning trees (Fig. 2A). These key genes were found to be significantly expressed in the virus response with respect to sham and exhibited significant expression differences between T1L (T1) and T3D-RV (T3) in the indicated tissue types.

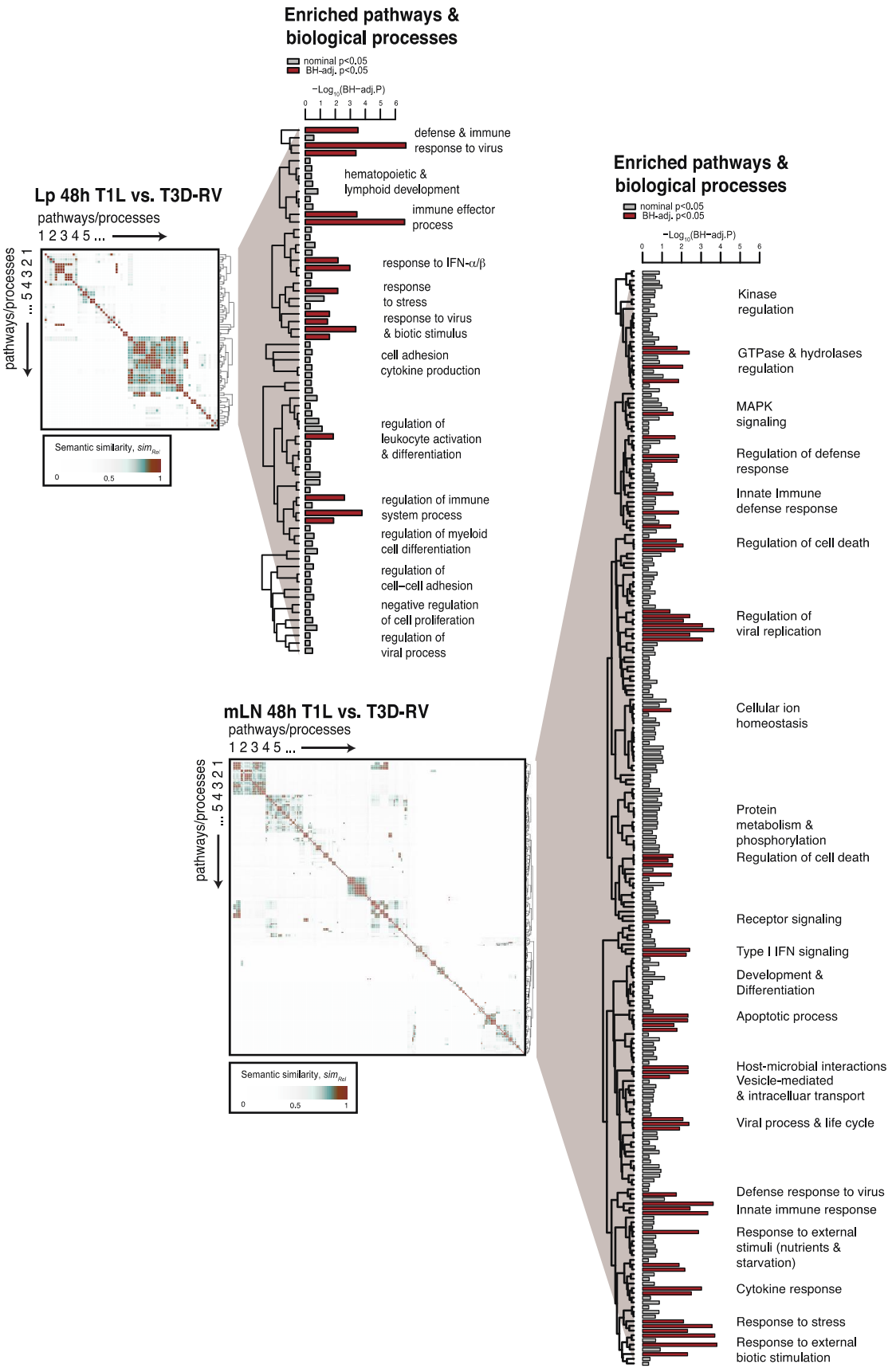
Enriched pathways & biological processes
nominal p<0.05
BH-adj. p<0.05
−Log10(BH−adj.P)
0 1 2 3 4 5 6
defense & immune response to virus
hematopoietic & lymphoid development
immune effector process
response to IFN-α/β
response to stress
response to virus & biotic stimulus
cell adhesion cytokine production
regulation of leukocyte activation & differentiation
regulation of immune system process
regulation of myeloid cell differentiation
regulation of cell–cell adhesion
negative regulation of cell proliferation
regulation of viral process
Lp 48h T1L vs. T3D-RV
pathways/processes
1 2 3 4 5 ...
pathways/processes
... 5 4 3 2 1
Semantic similarity, sim_Rel
0 0.5 1
mLN 48h T1L vs. T3D-RV
pathways/processes
1 2 3 4 5 ...
pathways/processes
... 5 4 3 2 1
Semantic similarity, sim_Rel
0 0.5 1
Enriched pathways & biological processes
nominal p<0.05
BH-adj. p<0.05
−Log10(BH−adj.P)
0 1 2 3 4 5 6
Kinase regulation
GTPase & hydrolases regulation
MAPK signaling
Regulation of defense response
Innate Immune defense response
Regulation of cell death
Regulation of viral replication
Cellular ion homeostasis
Protein metabolism & phosphorylation
Regulation of cell death
Receptor signaling
Type I IFN signaling
Development & Differentiation
Apoptotic process
Host-microbial interactions
Vesicle-mediated & intracelluar transport
Viral process & life cycle
Defense response to virus
Innate immune response
Response to external stimuli (nutrients & starvation)
Cytokine response
Response to stress
Response to external biotic stimulation

Fig. S3.

Enrichment analysis of pathway and biological processes enriched among differentially expressed genes between T1L and T3D-RV infected mice. Pathways or biological processes found enriched among genes that were differentially expressed between T1L and T3D-RV in lamina propria (Lp) or mLN were grouped on the basis of their relatedness by performing semantic similarity analysis using the relevance similarity measure, sim_{Rel} (scale ranging from 0 to 1, with 0 being distinct and 1 being identical). The analysis examines each pair of enriched pathway or process in turn and a semantic similarity matrix of sim_{Rel} values was constructed. From this analysis, a semantic cluster heatmap was generated and hierarchical clustering was applied to group similar pathways and processes together. The extent of similarity between pathways and processes scales with color intensity on the heatmap. Bar graphs showing enrichment scores ($-Log_{10}$(BH-adj.P)) associated with each pathway and process are shown. All meet the nominal (unadjusted) enrichment significance threshold of $P < 0.05$ as denoted by the grey bars. Red bars denote those achieving enrichment significance after Benjamini-Hochberg adjustment (BH-adj.$P < 0.05$) to control for the false discovery rate. Clusters of similar pathways and processes are grouped as indicated by dendrograms, and annotated by shared concepts.

A

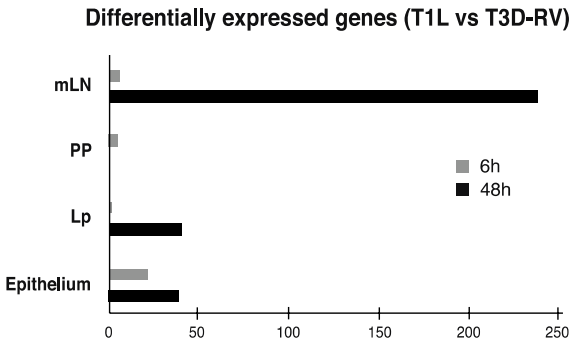

B

Early (6h)

	Epithelium	Lp	PP	mLN
T1L vs. Sham	190 (122)	99 (97)	267 (204)	77 (64)
T3D-RV vs. Sham	143 (120)	117 (97)	87 (85)	4 (4)

Late (48h)

	Epithelium	Lp	PP	mLN
T1L vs. Sham	109 (75)	114 (73)	289 (168)	1534 (691)
T3D-RV vs. Sham	87 (74)	76 (50)	254 (153)	607 (268)

Fig. S4.
Quantitation of differentially expressed genes between T1L and T3D-RV infected mice at inductive and effector sites of the gut (**A**) Bar plot showing the number of genes differentially expressed between T1L and T3D-RV infection in the respective tissues analyzed at 6 or 48 hpi as indicated. (**B**) Number of genes found to be differentially expressed between reovirus and sham-infected mice in the respective tissues as indicated (Benjamini-Hochberg-adjusted $P < 0.05$ and Fold-change > 1.5). Numbers in parentheses indicate up-regulated genes.

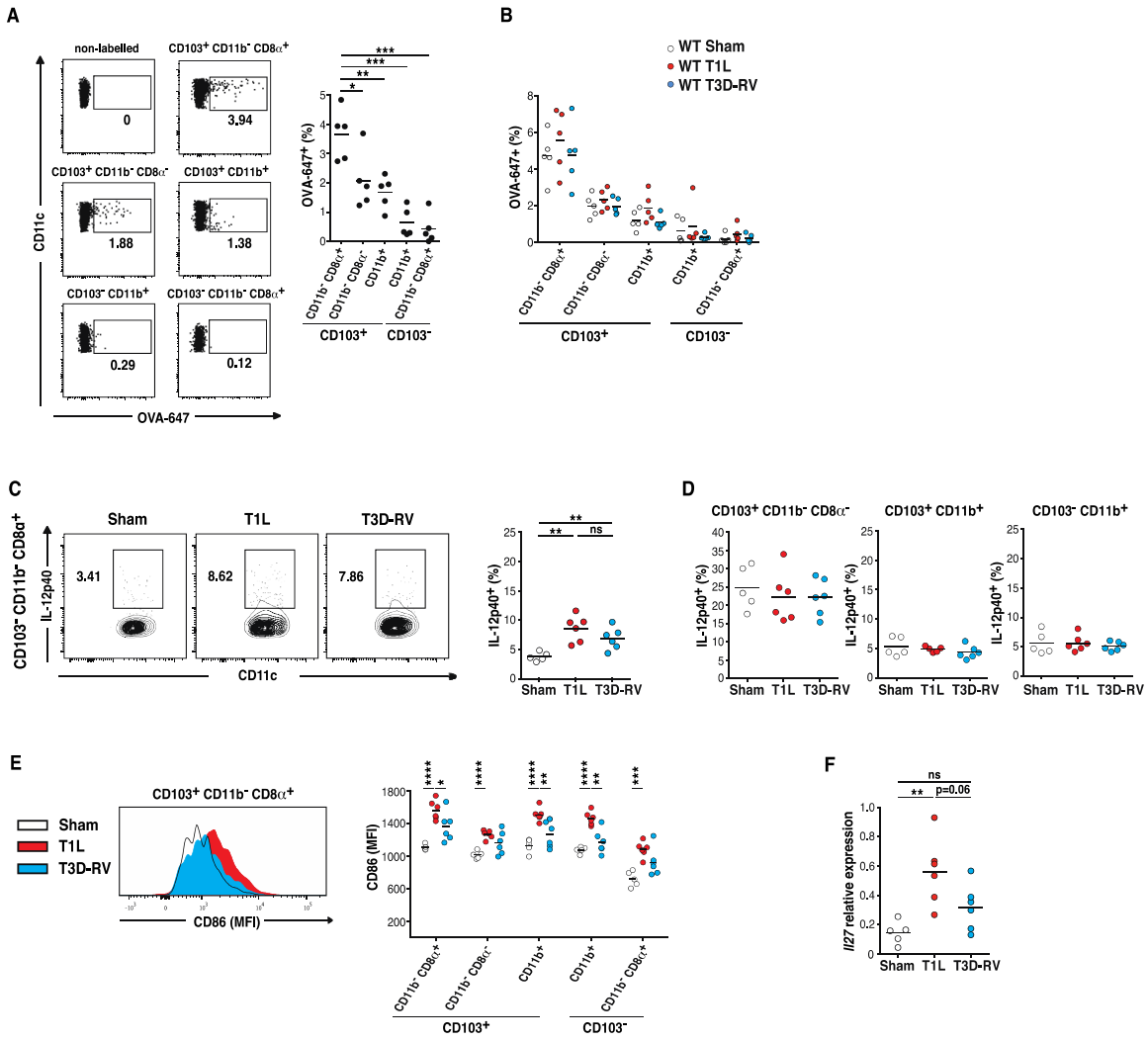

Fig. S5.

Dendritic cell (DC) activation and ovalbumin (OVA) uptake upon reovirus infection

(**A**) WT mice (n = 5) were gavaged with OVA-Alexa Fluor-647 18 hours before euthanasia and OVA-Alexa Fluor-647 uptake by DCs in the mLN was analyzed by flow cytometry. Representative dot plots and percentages of OVA-Alexa Fluor-647 uptake are shown in the indicated DC subsets. (**B**) Similar to (A) but mice were inoculated with 10^8 PFU of T1L (n = 5), 10^8 PFU of T3D-RV (n = 5), or PBS (sham, n = 5) at the time of gavaging with OVA-Alexa Fluor-647. (**C** to **F**) WT mice were inoculated perorally with 10^8 PFU of T1L (n = 6), 10^8 PFU of T3D-RV (n = 6), or PBS (sham, n = 5) for 2 days. (C and D) The expression of IL-12p40 in mLN DC subsets was evaluated by flow cytometry. Representative dot plots (C) and percentages (C and D) of IL-12p40$^+$ cells in indicated mLN DC subsets are shown. (E) The expression of CD86 in mLN DC subsets was evaluated by flow cytometry. Representative histogram and MFI for CD86 expression in the indicated DC subsets in the mLN of WT mice is shown. (F) *Il27* expression in the mLN 2dpi was analyzed by RT-PCR. (A to F) Graphs depict two independent experiments. *P < 0.05, **P < 0.01, ***P < 0.001, ****P < 0.0001 (One-way ANOVA / Tukey's multiple comparison).

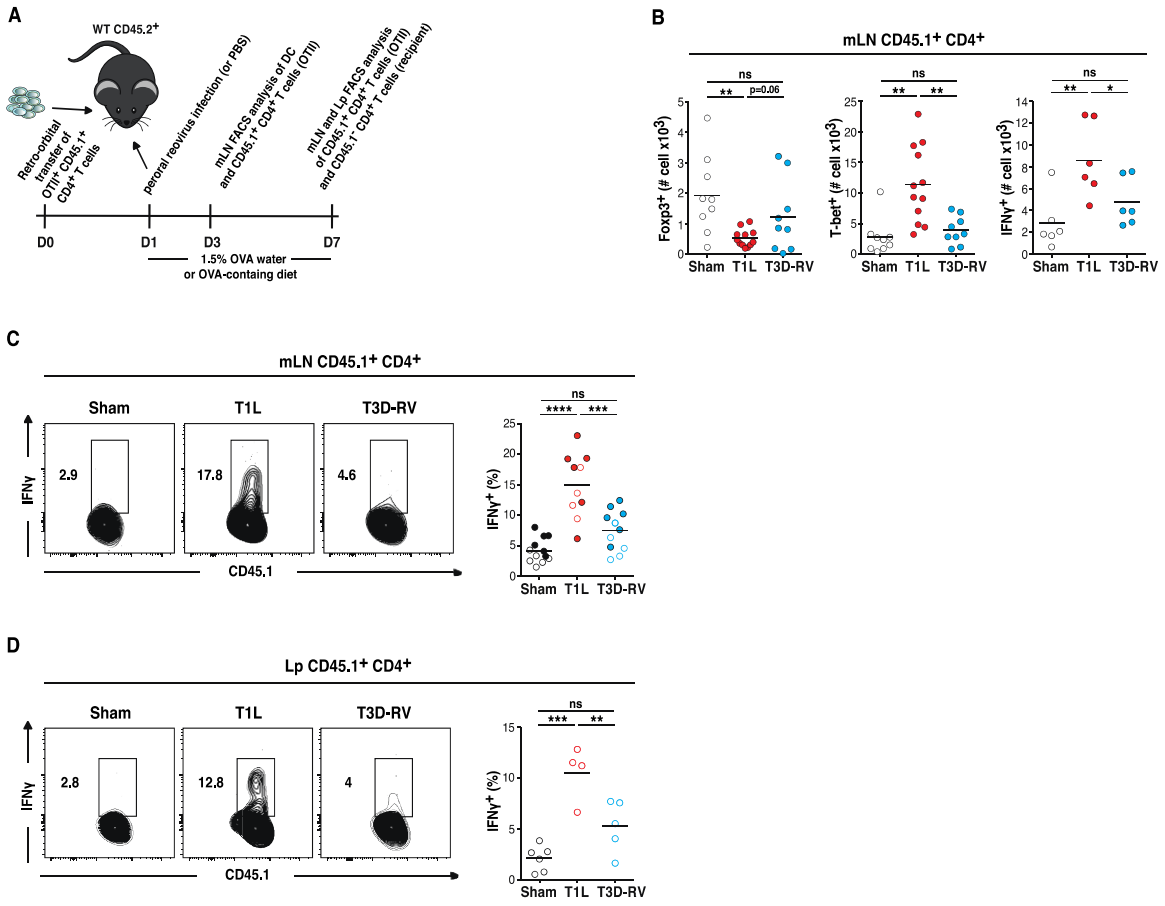

Fig. S6.

T1L promotes T_H1 immunity to dietary antigen at inductive and effector sites of the gut (**A**) *In vivo* T cell conversion assay model. (**B**) OT-II$^+$ CD45.1$^+$ CD4$^+$ T cells were transferred into WT CD45.2$^+$ mice. One day after transfer, mice were inoculated perorally with 10^{10} PFU of T1L (n = 6-12), 10^{10} PFU of T3D-RV (n = 6-9), or PBS (sham, n = 6-9) and fed 1.5% OVA in the drinking water for 6 days. The intracellular expression of Foxp3, T-bet, and IFNγ in mLN OT-II$^+$ CD45.1$^+$ CD4$^+$ T cells was evaluated by flow cytometry. Absolute numbers of Foxp3-, T-bet- and IFNγ-expressing CD45.1$^+$ CD4$^+$ T cells are shown. (**C** and **D**) OT-II$^+$ CD45.1$^+$ CD4$^+$ T cells isolated by MACS beads separation (filled circles) or FACS sorting (open circles) were transferred into WT CD45.2$^+$ mice. One day after transfer, mice were inoculated perorally with 10^{10} PFU of T1L (n = 4-16), 10^{10} PFU of T3D-RV (n = 5-14), or PBS (sham, n = 6-15) and fed 1.5% OVA in the drinking water (filled circles) or an OVA-containing diet (open circles) for 6 days. The intracellular expression of IFNγ in transferred OT-II$^+$ CD45.1$^+$ CD4$^+$ T cells in the mLN and in the Lp was evaluated by flow cytometry. Representative dot plots and percentages of IFNγ-producing CD45.1$^+$ CD4$^+$ T cells are shown in mLN (C) and in Lp (D) respectively. (B to D) Graphs depict at least two independent experiments. *P < 0.05, **P < 0.01, ***P < 0.001, ****P < 0.0001 (One-way ANOVA / Tukey's multiple comparison).

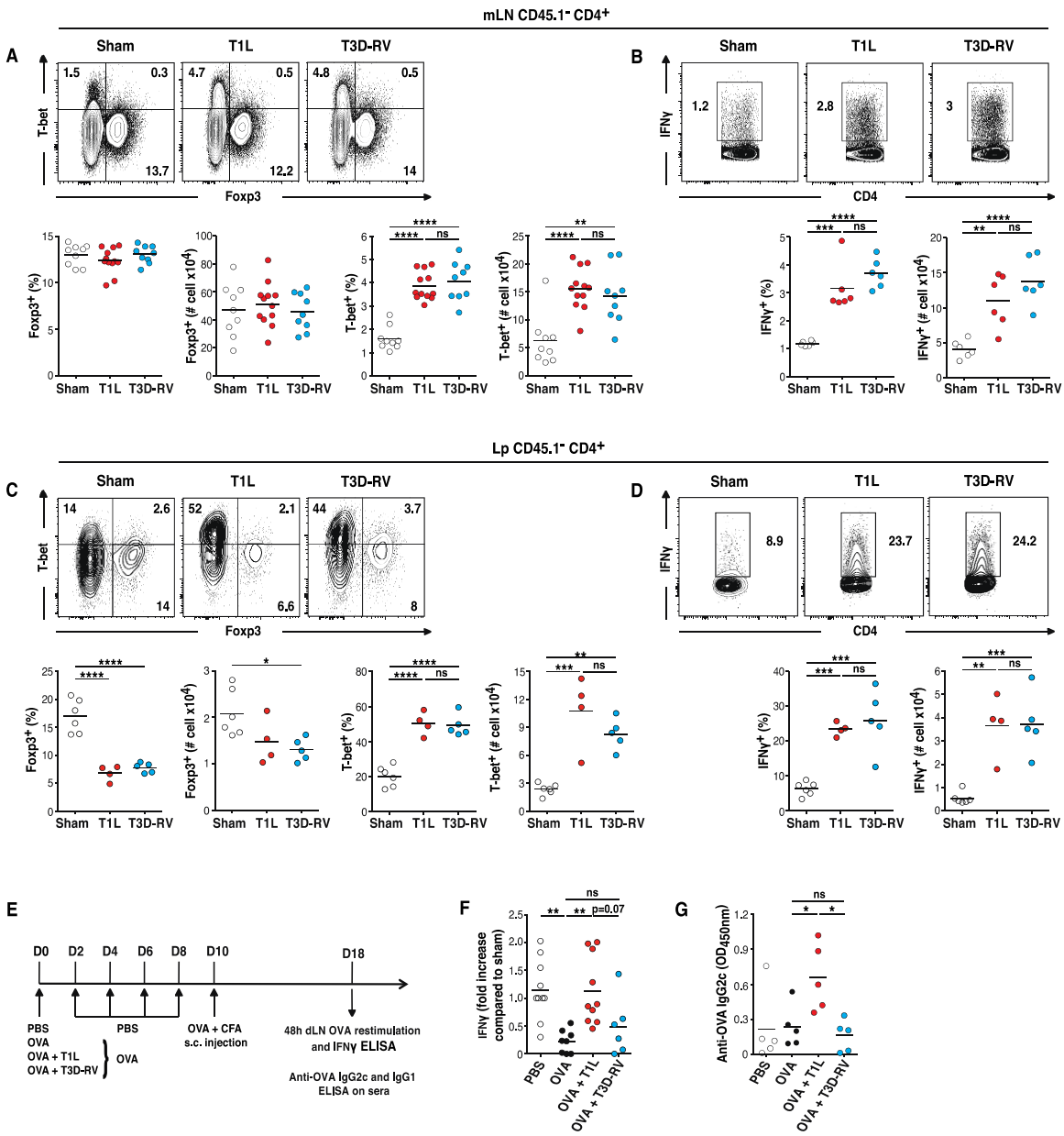

Fig. S7.

T cell responses to dietary antigen and viral infection (**A** and **B**) OT-II^{+} CD45.1^{+} CD4^{+} T cells were transferred into WT CD45.2^{+} mice. One day after transfer, mice were inoculated perorally with 10^{10} PFU of T1L (n = 6-12), 10^{10} PFU of T3D-RV (n = 6-9), or PBS (sham, n = 6-9) and fed 1.5% OVA in the drinking water for 6 days. The intracellular expression of Foxp3, T-bet, and IFNγ in mLN CD4^{+} T cells was evaluated by flow cytometry. Representative dot plots, percentages and absolute numbers of Foxp3-, T-bet- (A) and IFNγ-expressing CD45.1^{-} recipient CD4^{+} T cells (B) are shown. (**C** and **D**) OT-II^{+} CD45.1^{+} CD4^{+} T cells were transferred into WT CD45.2^{+} mice. One day after transfer, mice were inoculated perorally with 10^{10} PFU of T1L (n = 4), 10^{10} PFU of T3D-RV (n = 5), or PBS (sham, n = 6) and fed with an OVA-containing diet for 6 days. The

intracellular expression of Foxp3, T-bet and IFNγ in Lp $CD4^+$ T cells was evaluated by flow cytometry. Representative dot plots, percentages and absolute numbers of Foxp3-, T-bet- (C) and IFNγ-expressing $CD45.1^-$ recipient $CD4^+$ T cells (D) are shown. (**E** and **F**) WT mice were inoculated perorally with 10^{10} PFU of T1L, or 10^{10} PFU of T3D-RV, or PBS at the initiation of an oral tolerance protocol. Mice were gavaged every other day with OVA or PBS for 8 days and all mice were immunized subcutaneously (s.c) with OVA-CFA at 10 dpi. On day 18, draining lymph node (dLN) cells were harvested and analyzed for production of IFNγ by ELISA following OVA *in vitro* restimulation. Sham (n = 11), OVA (n = 11), OVA + T1L (n = 10), and OVA + T3D-RV (n = 6). (**G**) WT mice were inoculated perorally with 10^{10} PFU of T1L, 10^{10} PFU of T3D-RV, or PBS at the initiation of an oral tolerance protocol. Mice were fed with an OVA-containing diet or a control diet (sham) for 8 days and then immunized subcutaneously with OVA-CFA at 10 dpi. The levels of OVA-specific IgG2c antibodies were evaluated in the serum at day 18 by ELISA. Sham (n = 5), OVA (n = 5), OVA + T1L (n = 5), and OVA + T3D-RV (n = 5). (A to D and F and G) Graphs depict at least two independent experiments. *P < 0.05, **P < 0.01, ***P < 0.001, ****P < 0.0001 (One-way ANOVA / Tukey's multiple comparison).

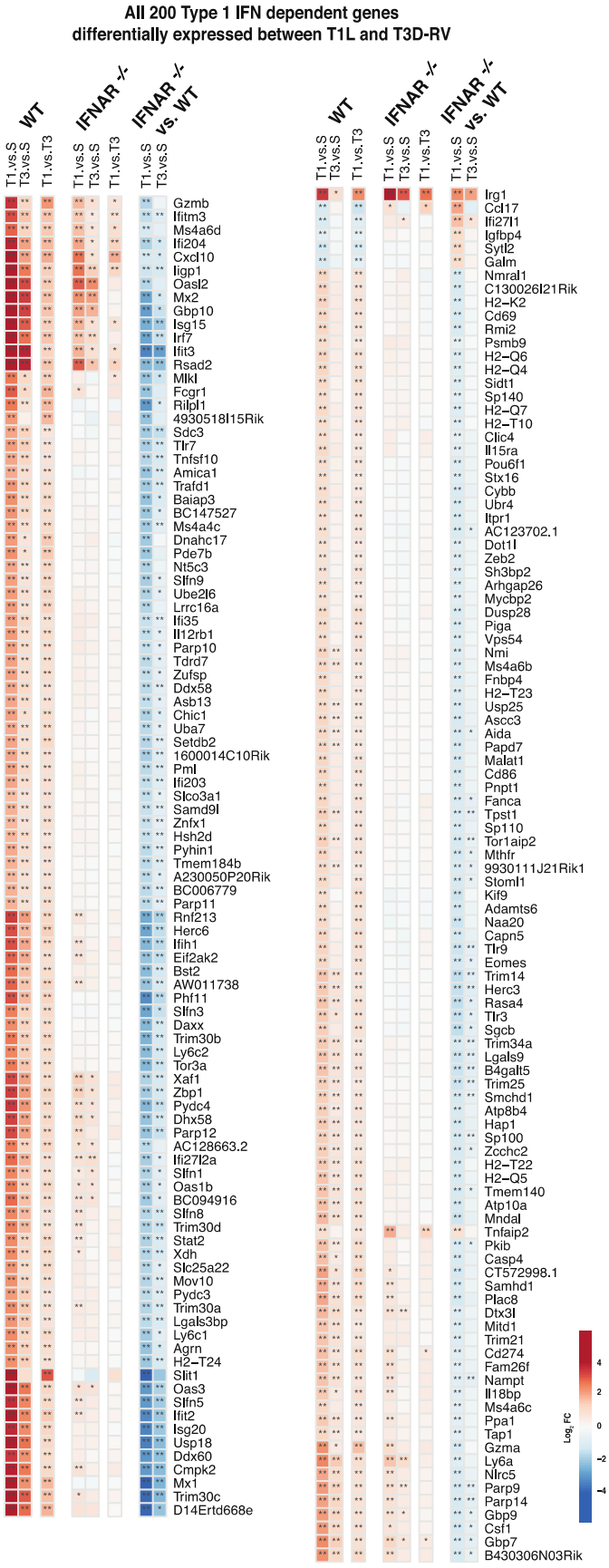
All 200 Type 1 IFN dependent genes
differentially expressed between T1L and T3D-RV
WT
IFNAR -/-
IFNAR -/- vs. WT
T1.vs.S
T3.vs.S
T1.vs.T3
Gzmb
Ifitm3
Ms4a6d
Ifi204
Cxcl10
Iigp1
Oasl2
Mx2
Gbp10
Isg15
Irf7
Ifit3
Rsad2
Mkl
Fcgr1
Rilpl1
4930518I15Rik
Sdc3
Tlr7
Tnfsf10
Amica1
Trafd1
Baiap3
BC147527
Ms4a4c
Dnahc17
Pde7b
Nt5c3
Slfn9
Ube2l6
Lrrc16a
Ifi35
Il12rb1
Parp10
Tdrd7
Zufsp
Ddx58
Asb13
Chic1
Uba7
Setdb2
1600014C10Rik
Pml
Ifi203
Slco3a1
Samd9l
Znfx1
Hsh2d
Pyhin1
Tmem184b
A230050P20Rik
BC006779
Parp11
Rnf213
Herc6
Ifih1
Eif2ak2
Bst2
AW011738
Phf11
Slfn3
Daxx
Trim30b
Ly6c2
Tor3a
Xaf1
Zbp1
Pydc4
Dhx58
Parp12
AC128663.2
Ifi27l2a
Slfn1
Oas1b
BC094916
Slfn8
Trim30d
Stat2
Xdh
Slc25a22
Mov10
Pydc3
Trim30a
Lgals3bp
Ly6c1
Agrn
H2−T24
Slit1
Oas3
Slfn5
Ifit2
Isg20
Usp18
Ddx60
Cmpk2
Mx1
Trim30c
D14Ertd668e
Irg1
Ccl17
Ifi27l1
Igfbp4
Sytl2
Galm
Nmral1
C130026I21Rik
H2−K2
Cd69
Rmi2
Psmb9
H2−Q6
H2−Q4
Sidt1
Sp140
H2−Q7
H2−T10
Clic4
Il15ra
Pou6f1
Stx16
Cybb
Ubr4
Itpr1
AC123702.1
Dot1l
Zeb2
Sh3bp2
Arhgap26
Mycbp2
Dusp28
Piga
Vps54
Nmi
Ms4a6b
Fnbp4
H2−T23
Usp25
Ascc3
Aida
Papd7
Malat1
Cd86
Pnpt1
Fanca
Tpst1
Sp110
Tor1aip2
Mthfr
9930111J21Rik1
Stoml1
Kif9
Adamts6
Naa20
Capn5
Tlr9
Eomes
Trim14
Herc3
Rasa4
Tlr3
Sgcb
Trim34a
Lgals9
B4galt5
Trim25
Smchd1
Atp8b4
Hap1
Sp100
Zcchc2
H2−T22
H2−Q5
Tmem140
Atp10a
Mndal
Tnfaip2
Pkib
Casp4
CT572998.1
Samhd1
Plac8
Dtx3l
Mitd1
Trim21
Cd274
Fam26f
Nampt
Il18bp
Ms4a6c
Ppa1
Tap1
Gzma
Ly6a
Nlrc5
Parp9
Parp14
Gbp9
Csf1
Gbp7
B430306N03Rik
Log2 FC
4
2
0
−2
−4

Fig. S8.

Type-1 IFN dependent genes differentially expressed between T1L and T3D-RV

WT and IFNAR$^{-/-}$ mice were inoculated perorally with 10^8 PFU of T1L (n = 3), 10^8 PFU of T3D-RV (n = 3), or PBS (sham, n = 3) and euthanized at 2 dpi. RNA of mLN was isolated for RNA-sequencing analysis. Heatmap showing type-1 IFN-dependent genes differentially expressed between T1L and T3D-RV. In the sections indicated as "WT" or "IFNAR$^{-/-}$", the heatmap shows genes that are statistically differentially expressed in T1L versus sham (T1. vs. S), T3D-RV versus sham (T3. vs. S), and T1L (with respect to sham) versus T3D-RV (with respect to sham) (T1. vs. T3) in both WT and IFNAR$^{-/-}$ mLN. An additional factorial design analysis in the section marked "IFNAR$^{-/-}$ vs. WT" examines the "differential-of-differential" expression, i.e., the transcriptional response differences to each virus in IFNAR$^{-/-}$ versus WT mLN: (T1. vs. S in IFNAR$^{-/-}$) versus (T1. vs. S in WT), or (T3. vs. S in IFNAR$^{-/-}$) versus (T3. vs. S in WT). Genes with expression levels found to be significantly different between IFNAR$^{-/-}$ and WT by factorial design analysis were identified as type-1 IFN-dependent. **denotes Benjamini-Hochberg-adjusted $P < 0.05$, *denotes nominal $P < 0.05$.

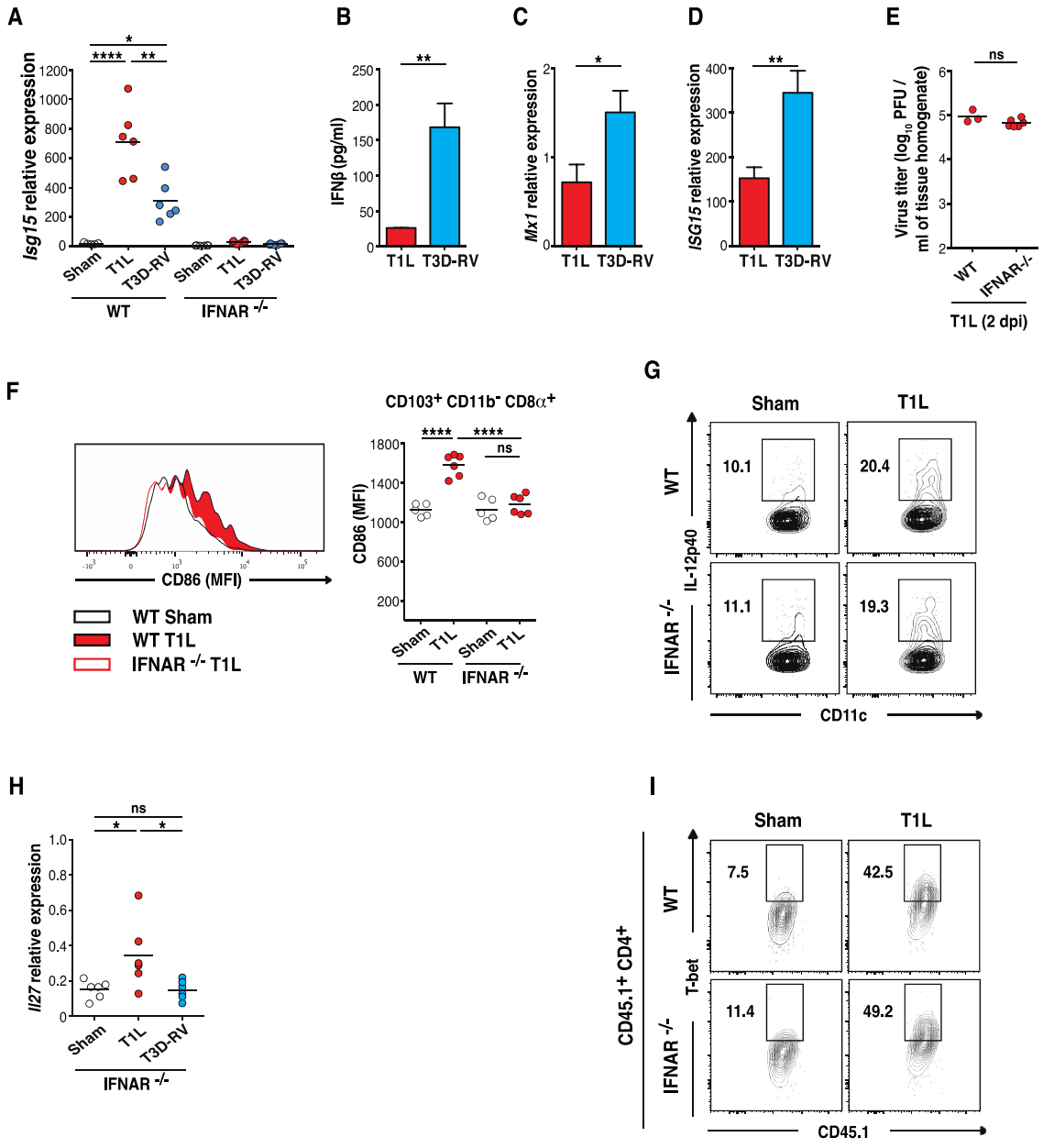

Fig. S9.

Impact of type-1 IFN signaling on the response to dietary antigen (**A**) WT and IFNAR$^{-/-}$ mice were inoculated perorally with 10^8 PFU of T1L (n = 6), 10^8 PFU of T3D-RV (n = 6) or PBS (sham, n = 6) and euthanized at 2 dpi. *ISG15* expression in the mLN was analyzed by RT-PCR. (**B**) IFNβ protein expression was analyzed by ELISA in WT mouse embryonic fibroblasts (MEFs) 16 hpi with T1L or T3D-RV at an MOI of 500 PFU/cell. (**C** and **D**) *Mx1* and *Isg15* mRNA levels were quantified by RT-PCR in Caco-2 cells 24 hpi with T1L or T3D-RV at an MOI of 100 PFU/cell. (**E**) OT-II$^+$ CD45.1$^+$ CD4$^+$ T cells were transferred into WT CD45.2$^+$ or IFNAR$^{-/-}$ CD45.2$^+$ mice. One day after transfer, mice were inoculated perorally with 10^8 PFU of T1L and fed 1.5% OVA in the drinking water for 2 days. At 2 dpi, a 1 cm section of ileum was resected, and viral titers

in WT (n = 3) and IFNAR$^{-/-}$ (n = 6) tissue were determined by plaque assay and expressed as PFU per ml of tissue homogenate. (**F, G** and **I**) OT-II^{+} CD45.1^{+} CD4^{+} T cells were transferred into WT CD45.2^{+} or IFNAR$^{-/-}$ CD45.2^{+} mice. One day after transfer, mice were inoculated perorally with 10^8 PFU of T1L or PBS (sham) and fed 1.5% OVA in the drinking water for 2 days. The expression of CD86 (F) IL-12p40 (G) and T-bet (I) in the mLN was evaluated by flow cytometry. (F) Representative histogram and MFI of the expression of CD86 is shown in CD103^{+} CD11b^{-} CD8α^{+} DCs in the mLN. (G) Representative dot plots of mLN IL-12p40-producing CD103^{+} CD11b^{-} CD8α^{+} DCs are shown. (I) Representative dot plots of mLN T-bet-expressing OT-II^{+} CD45.1^{+} CD4^{+} T cells are shown. (**H**) IFNAR$^{-/-}$ mice were inoculated perorally with 10^8 PFU of T1L (n = 6), 10^8 PFU of T3D-RV (n = 6), or PBS (sham, n = 6) and were euthanized at 2 dpi. *Il27* expression in the mLN was analyzed by RT-PCR. (A to I) Graphs depict two independent experiments. (A, F and H) *P < 0.05, **P < 0.01, ***P < 0.001, ****P < 0.0001 (One-way ANOVA / Tukey's multiple comparison). (B to E) *P < 0.05, **P < 0.01 (unpaired t-test).

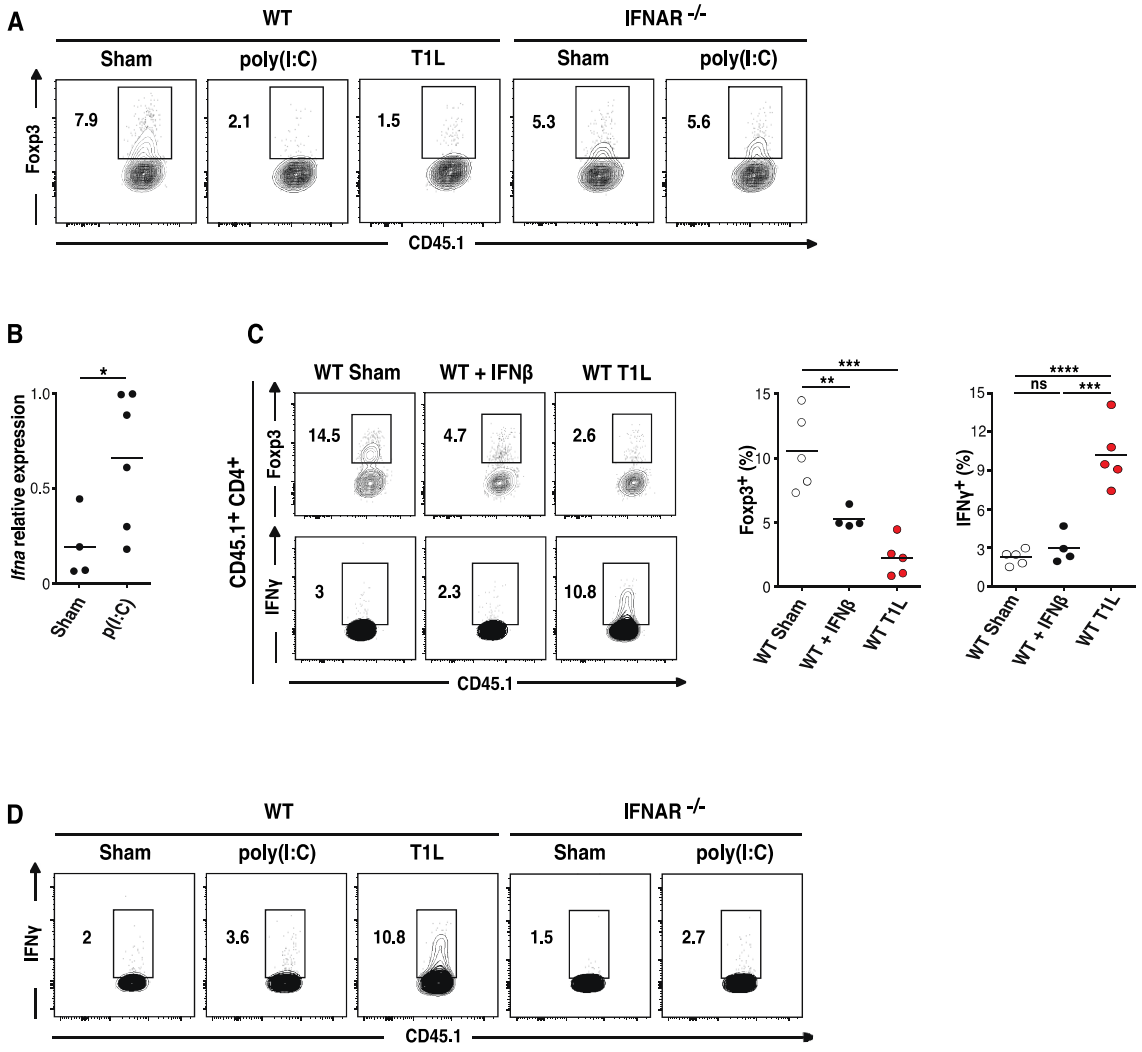

Fig. S10.

dsRNA is sufficient to block pTreg conversion in a type-1 IFN-dependent manner (**A** and **D**) OT-II^{+} CD45.1^{+} CD4^{+} T cells were transferred into WT CD45.2^{+} or IFNAR$^{-/-}$ CD45.2^{+} mice. One day after transfer, mice were inoculated with PBS (n = 7) or 50 μg of poly(I:C) (n = 7) i.p. or 10^{10} PFU of T1L (n = 5) perorally, and fed an OVA-containing diet for 6 days. The intracellular expression of Foxp3 and IFNγ in OT-II^{+} CD45.1^{+} CD4^{+} T cells in the mLN was evaluated by flow cytometry. Representative dot plots of Foxp3- (A) and IFNγ-expressing CD45.1^{+} CD4^{+} T cells (D) are shown. (**B**) WT mice were inoculated with PBS (sham, n = 4) or 50 μg of poly(I:C) (n = 6) i.p. and euthanized 2 days post injection. *Ifnα* expression in the mLN was evaluated by RT-PCR. (**C**) OT-II^{+} CD45.1^{+} CD4^{+} T cells were transferred into WT CD45.2^{+} mice. One day after transfer, mice received PBS (sham, n = 5) or IFNβ (n = 4) i.p. or were inoculated perorally with 10^{10} PFU of T1L (n = 5), and fed an OVA-containing diet for 6 days. The intracellular expression of Foxp3 and IFNγ in OT-II^{+} CD45.1^{+} CD4^{+} T cells in the mLN was evaluated by flow cytometry. Representative dot plots and percentages of Foxp3- and IFNγ-expressing CD45.1^{+} CD4^{+} T cells are shown. (B and C) Graphs depict two independent experiments. (B) *P < 0.05 (unpaired t-test). (C) **P < 0.01, ***P < 0.001, ****P < 0.0001 (One-way ANOVA / Tukey's multiple comparison).

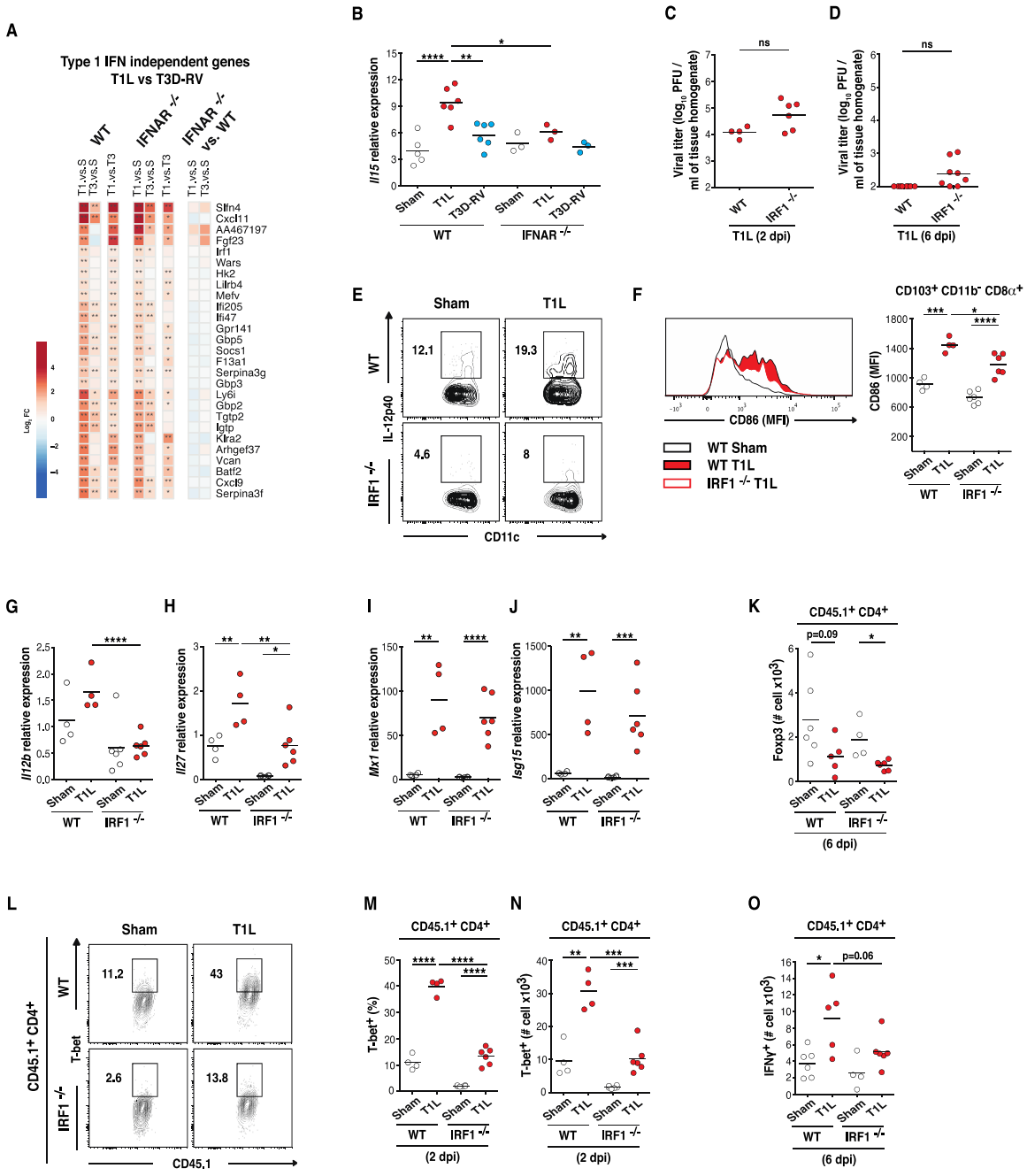

Fig. S11.

Role of IRF1 signaling in the response to dietary antigens upon reovirus infection (**A**) WT and IFNAR$^{-/-}$ mice were inoculated perorally with 10^8 PFU of T1L (n = 3), 10^8 PFU of T3D-RV (n = 3), or PBS (sham, n = 3) and euthanized at 2 dpi. RNA of mLN was isolated for RNA-seq analysis. Heatmap showing genes differentially expressed between T1L and T3D-RV in a type-1 IFN-independent manner. Differential transcriptional responses for T1L versus sham (T1. vs. S), T3D-RV versus sham (T3. vs.

S), and T1L (with respect to sham) versus T3D-RV (with respect to sham) (T1. vs. T3) are shown in sub-sections labeled "WT" or "IFNAR$^{-/-}$". Factorial design analysis indicates no statistical difference between IFNAR$^{-/-}$ and WT mLN (third sub-section labeled "IFNAR$^{-/-}$ vs. WT") for these genes. **denotes Benjamini-Hochberg-adjusted P < 0.05, *denotes nominal P < 0.05. (**B**) WT and IFNAR$^{-/-}$ mice were inoculated perorally with 10^8 PFU of T1L, 10^8 PFU of T3D-RV or PBS (sham) and euthanized at 2 dpi. *Il15* expression in the mLN was analyzed by RT-PCR. WT sham (n = 5), WT T1L (n = 6), WT T3D-RV (n = 6), IFNAR$^{-/-}$ sham (n = 3), IFNAR$^{-/-}$ T1L (n = 3), and IFNAR$^{-/-}$ T3D-RV (n = 3). (**C, E, F, L** to **N**) OT-II$^+$ CD45.1$^+$ CD4$^+$ T cells were transferred into WT CD45.2$^+$ or IRF1$^{-/-}$ CD45.2$^+$ mice. One day after transfer, mice were inoculated perorally with 10^8 PFU of T1L or PBS (sham) and fed 1.5% OVA in the drinking water for 2 days. (C) At 2 dpi, a 1cm section of ileum was resected, and viral titers in this tissue were determined by plaque assay. (E, F, L to N) The expression of IL-12p40, CD86, and T-bet in the mLN was evaluated by flow cytometry. (E) Representative dot plots of mLN IL-12p40-producing CD103$^+$ CD11b$^-$ CD8α$^+$ DC are shown. (F) Representative histogram and MFI for CD86 expression in mLN CD103$^+$ CD11b$^-$ CD8α$^+$ DCs are shown. (L) Representative dot plots, (M) percentages and, (N) absolute numbers of T-bet-expressing CD45.1$^+$ CD4$^+$ T cells are shown. **(D, K,** and **O)** OT-II$^+$ CD45.1$^+$ CD4$^+$ T cells were transferred into WT CD45.2$^+$ or IRF1$^{-/-}$ CD45.2$^+$ mice. One day after transfer, mice were inoculated perorally with 10^{10} PFU of T1L or PBS (sham) and fed 1.5% OVA in the drinking water for 6 days. (D) At 6 dpi, a 1cm section of ileum was resected, and viral titers in this tissue were determined by plaque assay. (K and O) Intracellular expressions of Foxp3 and IFNγ were evaluated by flow cytometry. Absolute numbers of Foxp3- (K) and IFNγ-expressing CD45.1$^+$ CD4$^+$ T cells (O) in the mLN are shown. WT sham (n = 6), WT T1L (n = 5), IRF1$^{-/-}$ sham (n = 4), and IRF1$^{-/-}$ T1L (n = 6). **(G** to **J)** WT and IRF1$^{-/-}$ mice were inoculated perorally with 10^8 PFU of T1L or PBS (sham) and euthanized at 2 dpi. (G) *Il12b,* (H) *Il27,* (I) *Mx1* and (J) *Isg15* expression in the mLN was analyzed by RT-PCR, WT sham (n = 4), WT T1L (n = 4), IRF1$^{-/-}$ sham (n = 6), IRF1$^{-/-}$ T1L (n = 6). (B to O) Graphs depict two independent experiments. (B, G to K, M to O) *P < 0.05, **P < 0.01, ***P < 0.001, ****P < 0.0001 (One-way ANOVA / Tukey's multiple comparison). (C and D) (unpaired t-test).

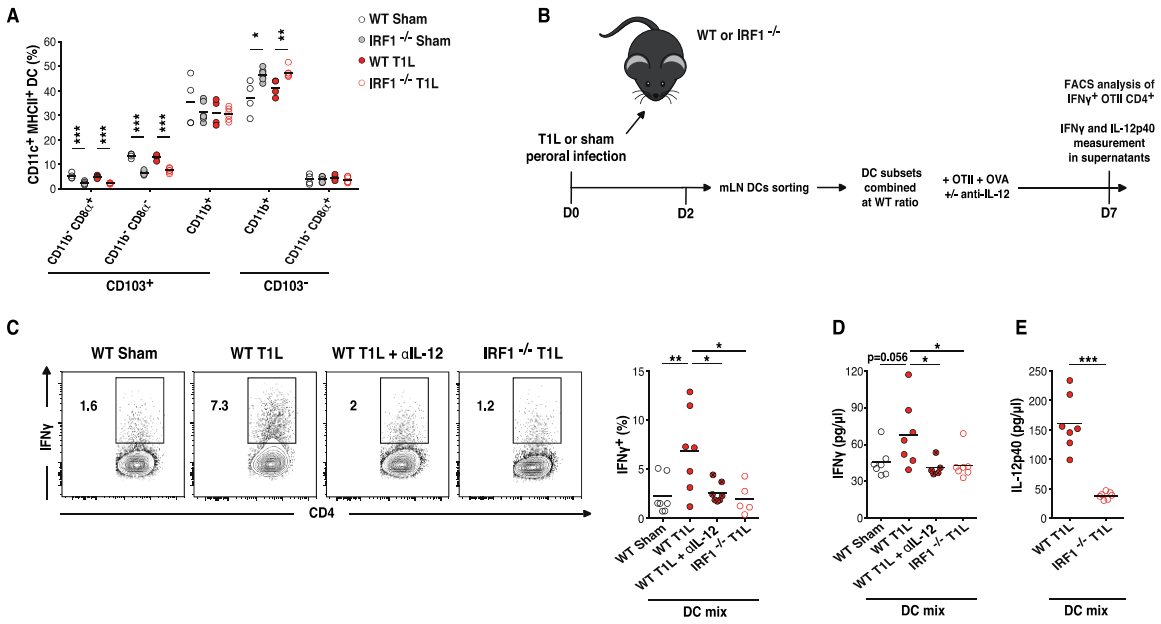

Fig. S12.

Role of IRF1 in dendritic cells (**A** to **E**) WT and IRF1$^{-/-}$ mice were inoculated perorally with 10^8 PFU of T1L or PBS (sham) and euthanized at 2 dpi. (A) The DC subsets distribution in the mLN was evaluated by flow cytometry. The percentages of each DC subset are indicated. WT sham (n = 4, open grey circles), WT T1L (n = 4, closed red circles), IRF1$^{-/-}$ sham (n = 5, closed grey circles), and IRF1$^{-/-}$ T1L (n = 5, open red circles). (B) The four major DC subsets (CD103$^+$ CD11b$^-$ CD8α$^+$, CD103$^+$ CD11b$^-$ CD8α$^-$, CD103$^+$ CD11b$^+$, CD103$^-$ CD11b$^+$) from WT or IRF1$^{-/-}$ mLN were FACS sorted and reconstituted at the WT ratio and incubated together with naïve OT-II$^+$ CD4$^+$ T cells for 5 days in presence of OVA with or without anti-IL12 neutralizing antibody. (C) Intracellular expression of IFNγ in OT-II CD4$^+$ T cells was evaluated by flow cytometry. Representative dot plots and percentages of IFNγ-expressing CD4$^+$ T cells are shown. (D and E) Levels of IFNγ and IL-12p40 in the co-culture supernatants were evaluated by BioPlex. (A and C to E) Graphs depict two independent experiments. (A and E) *P < 0.05, **P < 0.01, ***P < 0.001 (unpaired t-test). (C and D) *P < 0.05, **P < 0.01 (One-way ANOVA / Tukey's multiple comparison).

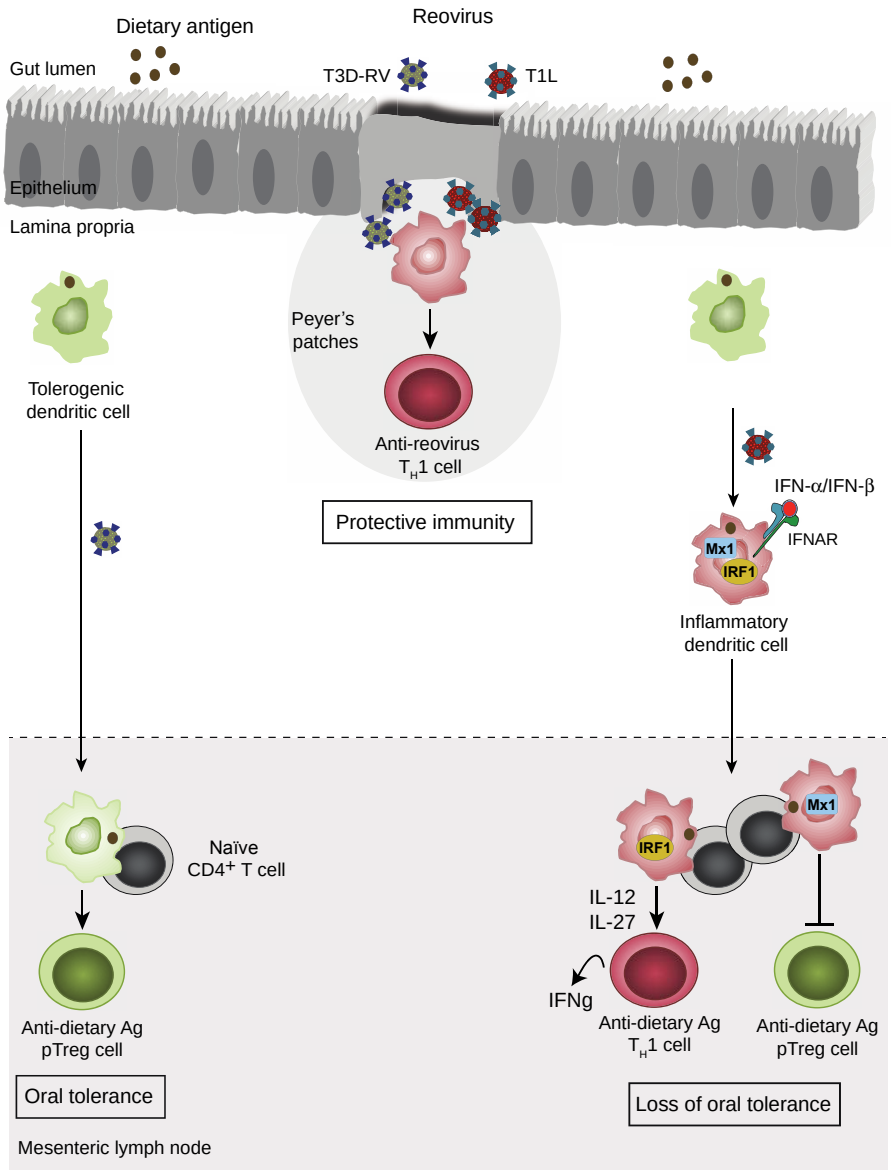

Fig. S13.
Two reoviruses similarly infect the intestine and induce protective immunity, but differ in their immunopathological outcomes.
Under homeostatic conditions, regulatory T cell responses to dietary antigen are induced in the small intestine (Oral tolerance). T1L and T3D-RV reoviruses induce immune responses in Peyer's patches, the site where protective immunity to reovirus is induced. In contrast, in mesenteric lymph nodes, the site of oral tolerance induction, T1L but not T3D-RV upregulates type-1 IFN signaling (Mx1; type-1 IFN induced gene; proxy for type-1 IFN) as well as IL-12 and IL-27 production by dendritic cells. Consequently, T1L but not T3D-RV infection inhibits the conversion of peripheral regulatory Foxp3$^+$ T cells (pTreg) and promotes development of T_H1 immunity to dietary antigen (Loss of oral tolerance). While type-1 IFN signaling (Mx1) in antigen-presenting cells plays a role in blocking pTreg conversion, IRF1 is required for the induction of IL-12 and IL-27, and the subsequent development of T_H1 immunity to dietary antigen.

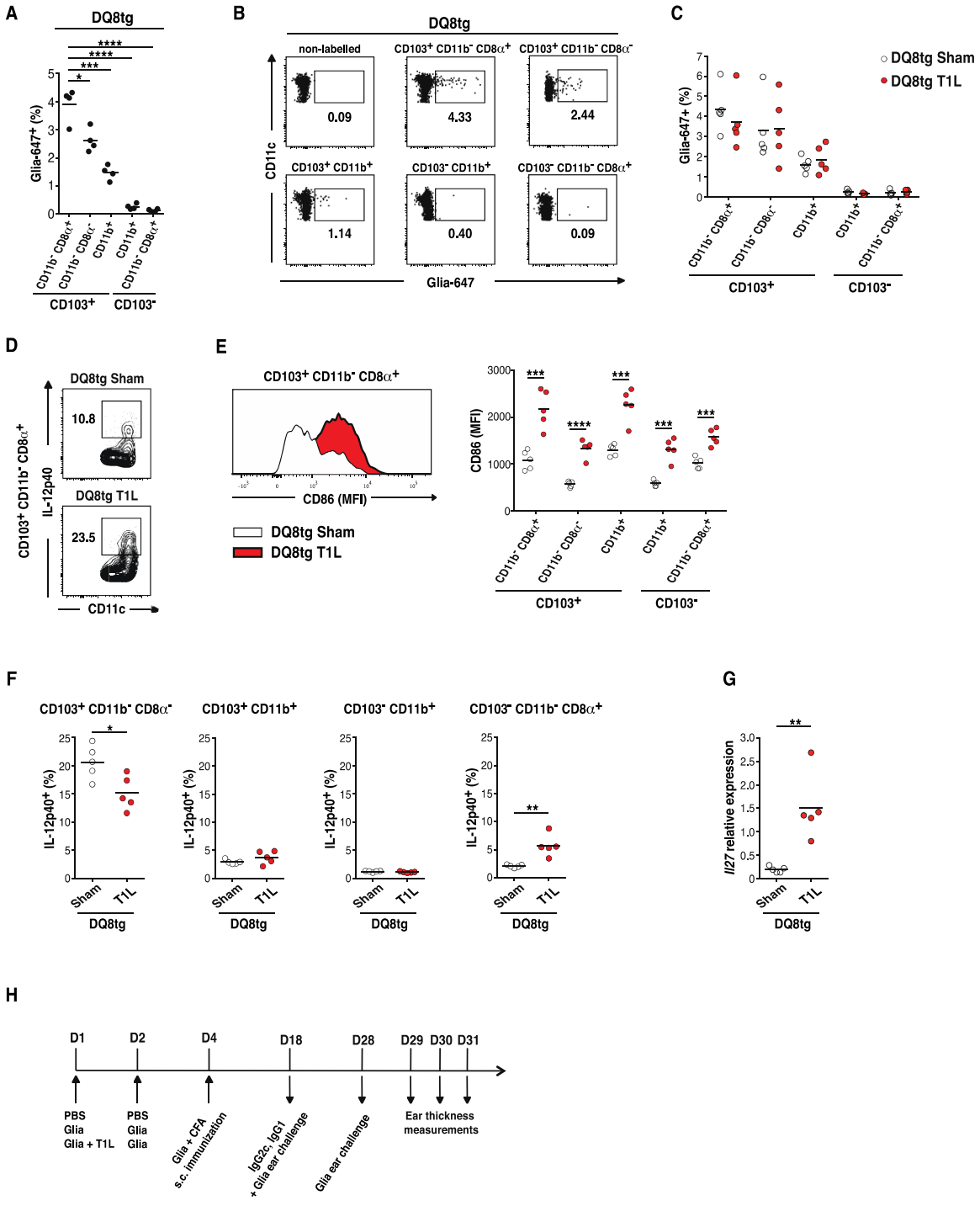

Fig. S14.

DC activation and gliadin uptake upon reovirus infection of DQ8tg mice (**A** and **B**) DQ8tg mice (n = 4) were gavaged with Alexa Fluor-647-labelled gliadin (Glia-Alexa

Fluor-647) 18h before euthanasia, and Glia-Alexa Fluor-647 uptake by DCs was analyzed by flow cytometry. (A) Percentages and (B) dot plots depicting Glia-Alexa Fluor-647 uptake by the indicated DC subsets are shown. (**C**) DQ8tg mice were gavaged with OVA-Alexa Fluor-647 and inoculated with 10^8 PFU of T1L (n = 5) or PBS (sham, n = 5). At 18 hpi, mice were euthanized, and Glia-Alexa Fluor-647 uptake by DCs in the mLN was analyzed by flow cytometry. Percentages of Glia-Alexa Fluor-647 uptake by the indicated DC subsets are shown. (**D** to **G)** DQ8tg mice were inoculated perorally with 10^8 PFU of T1L (n = 5) or PBS (sham, n = 5) and euthanized at 2 dpi. (D to F) The expression of IL-12p40 and CD86 in mLN DCs was evaluated by flow cytometry. (D) Representative dot plots of IL-12p40-producing $CD103^+$ $CD11b^-$ $CD8\alpha^+$ DCs are shown. (E) Representative histogram and MFI for CD86 expression and (F) percentage of mLN IL-12p40-producing DCs are shown. (G) *Il27* expression in the mLN was evaluated by RT-PCR. (**H**) Delayed type hypersensitivity (DTH) experimental design. (A to G) Graphs depict two independent experiments. (A) *P < 0.05, ***P < 0.001, ****P < 0.0001 (One-way ANOVA / Tukey's multiple comparison). (C and E to G) *P < 0.05, **P < 0.01, ***P < 0.001, ****P < 0.0001 (unpaired t-test).

References and Notes

1. V. Abadie, L. M. Sollid, L. B. Barreiro, B. Jabri, Integration of genetic and immunological insights into a model of celiac disease pathogenesis. *Annu. Rev. Immunol.* **29**, 493–525 (2011). doi:10.1146/annurev-immunol-040210-092915 Medline

2. J. M. Tjon, J. van Bergen, F. Koning, Celiac disease: How complicated can it get? *Immunogenetics* **62**, 641–651 (2010). doi:10.1007/s00251-010-0465-9 Medline

3. L. M. Sollid, B. Jabri, Triggers and drivers of autoimmunity: Lessons from coeliac disease. *Nat. Rev. Immunol.* **13**, 294–302 (2013). doi:10.1038/nri3407 Medline

4. E. M. Nilsen, F. L. Jahnsen, K. E. A. Lundin, F.-E. Johansen, O. Fausa, L. M. Sollid, J. Jahnsen, H. Scott, P. Brandtzaeg, Gluten induces an intestinal cytokine response strongly dominated by interferon gamma in patients with celiac disease. *Gastroenterology* **115**, 551–563 (1998). doi:10.1016/S0016-5085(98)70134-9 Medline

5. L. Shan, Ø. Molberg, I. Parrot, F. Hausch, F. Filiz, G. M. Gray, L. M. Sollid, C. Khosla, Structural basis for gluten intolerance in celiac sprue. *Science* **297**, 2275–2279 (2002). doi:10.1126/science.1074129 Medline

6. M. A. Curotto de Lafaille, J. J. Lafaille, Natural and adaptive foxp3^{+} regulatory T cells: More of the same or a division of labor? *Immunity* **30**, 626–635 (2009). doi:10.1016/j.immuni.2009.05.002 Medline

7. L. Plot, H. Amital, Infectious associations of celiac disease. *Autoimmun. Rev.* **8**, 316–319 (2009). doi:10.1016/j.autrev.2008.10.001 Medline

8. L. C. Stene, M. C. Honeyman, E. J. Hoffenberg, J. E. Haas, R. J. Sokol, L. Emery, I. Taki, J. M. Norris, H. A. Erlich, G. S. Eisenbarth, M. Rewers, Rotavirus infection frequency and risk of celiac disease autoimmunity in early childhood: A longitudinal study. *Am. J. Gastroenterol.* **101**, 2333–2340 (2006). doi:10.1111/j.1572-0241.2006.00741.x Medline

9. J. H. Tai, J. V. Williams, K. M. Edwards, P. F. Wright, J. E. Crowe Jr., T. S. Dermody, Prevalence of reovirus-specific antibodies in young children in Nashville, Tennessee. *J. Infect. Dis.* **191**, 1221–1224 (2005). doi:10.1086/428911 Medline

10. J. Angel, M. A. Franco, H. B. Greenberg, Rotavirus immune responses and correlates of protection. *Curr. Opin. Virol.* **2**, 419–425 (2012). doi:10.1016/j.coviro.2012.05.003 Medline

11. T. S. Dermody, J. S. Parker, B. Sherry, *Orthoreoviruses* (Lippincott Williams & Wilkins, ed. 6, 2013), pp. 1304–1346.

12. M. N. Fleeton, N. Contractor, F. Leon, J. D. Wetzel, T. S. Dermody, B. L. Kelsall, Peyer's patch dendritic cells process viral antigen from apoptotic epithelial cells in the intestine of reovirus-infected mice. *J. Exp. Med.* **200**, 235–245 (2004). doi:10.1084/jem.20041132 Medline

13. D. K. Bodkin, B. N. Fields, Growth and survival of reovirus in intestinal tissue: Role of the L2 and S1 genes. *J. Virol.* **63**, 1188–1193 (1989). Medline

14. A. J. Macpherson, K. Smith, Mesenteric lymph nodes at the center of immune anatomy. *J. Exp. Med.* **203**, 497–500 (2006). doi:10.1084/jem.20060227 Medline

15. O. Pabst, A. M. Mowat, Oral tolerance to food protein. *Mucosal Immunol.* **5**, 232–239 (2012). doi:10.1038/mi.2012.4 Medline

16. C. V. Cannistraci, T. Ravasi, F. M. Montevecchi, T. Ideker, M. Alessio, Nonlinear dimension reduction and clustering by Minimum Curvilinearity unfold neuropathic pain and tissue embryological classes. *Bioinformatics* **26**, i531–i539 (2010). doi:10.1093/bioinformatics/btq376 Medline

17. Y. Xu, V. Olman, D. Xu, Clustering gene expression data using a graph-theoretic approach: An application of minimum spanning trees. *Bioinformatics* **18**, 536–545 (2002). doi:10.1093/bioinformatics/18.4.536 Medline

18. J. L. Coombes, K. R. R. Siddiqui, C. V. Arancibia-Cárcamo, J. Hall, C.-M. Sun, Y. Belkaid, F. Powrie, A functionally specialized population of mucosal CD103$^+$ DCs induces Foxp3$^+$ regulatory T cells via a TGF-β and retinoic acid-dependent mechanism. *J. Exp. Med.* **204**, 1757–1764 (2007). doi:10.1084/jem.20070590 Medline

19. D. Esterházy, J. Loschko, M. London, V. Jove, T. Y. Oliveira, D. Mucida, Classical dendritic cells are required for dietary antigen-mediated induction of peripheral T_{reg} cells and tolerance. *Nat. Immunol.* **17**, 545–555 (2016). doi:10.1038/ni.3408 Medline

20. K. M. Luda, T. Joeris, E. K. Persson, A. Rivollier, M. Demiri, K. M. Sitnik, L. Pool, J. B. Holm, F. Melo-Gonzalez, L. Richter, B. N. Lambrecht, K. Kristiansen, M. A. Travis, M. Svensson-Frej, K. Kotarsky, W. W. Agace, IRF8 transcription-factor-dependent classical dendritic cells are essential for intestinal T cell homeostasis. *Immunity* **44**, 860–874 (2016). doi:10.1016/j.immuni.2016.02.008 Medline

21. R. Hinterleitner, B. Jabri, A dendritic cell subset designed for oral tolerance. *Nat. Immunol.* **17**, 474–476 (2016). doi:10.1038/ni.3435 Medline

22. M. Martínez-López, S. Iborra, R. Conde-Garrosa, D. Sancho, Batf3-dependent CD103+ dendritic cells are major producers of IL-12 that drive local Th1 immunity against Leishmania major infection in mice. *Eur. J. Immunol.* **45**, 119–129 (2015). doi:10.1002/eji.201444651 Medline

23. H. Yoshida, C. A. Hunter, The immunobiology of interleukin-27. *Annu. Rev. Immunol.* **33**, 417–443 (2015). doi:10.1146/annurev-immunol-032414-112134 Medline

24. M. A. van Leeuwen, L. M. M. Costes, L. A. van Berkel, Y. Simons-Oosterhuis, M. F. du Pré, A. E. Kozijn, H. C. Raatgeep, D. J. Lindenbergh-Kortleve, N. van Rooijen, F. Koning, J. N. Samsom, Macrophage-mediated gliadin degradation and concomitant IL-27 production drive IL-10- and IFN-γ-secreting Tr1-like-cell differentiation in a murine model for gluten tolerance. *Mucosal Immunol.* (2016). doi:10.1038/mi.2016.76 Medline

25. A. Di Sabatino, K. M. Pickard, J. N. Gordon, V. Salvati, G. Mazzarella, R. M. Beattie, A. Vossenkaemper, L. Rovedatti, N. A. B. Leakey, N. M. Croft, R. Troncone, G. R. Corazza, A. J. Stagg, G. Monteleone, T. T. MacDonald, Evidence for the role of interferon-α production by dendritic cells in the Th1 response in celiac disease. *Gastroenterology* **133**, 1175–1187 (2007). doi:10.1053/j.gastro.2007.08.018 Medline

26. S. C. Irvin, J. Zurney, L. S. Ooms, J. D. Chappell, T. S. Dermody, B. Sherry, A single-amino-acid polymorphism in reovirus protein μ2 determines repression of interferon

signaling and modulates myocarditis. *J. Virol.* **86**, 2302–2311 (2012). doi:10.1128/JVI.06236-11 Medline

27. C. Johansson, J. D. Wetzel, J. He, C. Mikacenic, T. S. Dermody, B. L. Kelsall, Type I interferons produced by hematopoietic cells protect mice against lethal infection by mammalian reovirus. *J. Exp. Med.* **204**, 1349–1358 (2007). doi:10.1084/jem.20061587 Medline

28. R. W. DePaolo, V. Abadie, F. Tang, H. Fehlner-Peach, J. A. Hall, W. Wang, E. V. Marietta, D. D. Kasarda, T. A. Waldmann, J. A. Murray, C. Semrad, S. S. Kupfer, Y. Belkaid, S. Guandalini, B. Jabri, Co-adjuvant effects of retinoic acid and IL-15 induce inflammatory immunity to dietary antigens. *Nature* **471**, 220–224 (2011). doi:10.1038/nature09849 Medline

29. T. Tamura, H. Yanai, D. Savitsky, T. Taniguchi, The IRF family transcription factors in immunity and oncogenesis. *Annu. Rev. Immunol.* **26**, 535–584 (2008). doi:10.1146/annurev.immunol.26.021607.090400 Medline

30. S. Taki, T. Sato, K. Ogasawara, T. Fukuda, M. Sato, S. Hida, G. Suzuki, M. Mitsuyama, E.-H. Shin, S. Kojima, T. Taniguchi, Y. Asano, Multistage regulation of Th1-type immune responses by the transcription factor IRF-1. *Immunity* **6**, 673–679 (1997). doi:10.1016/S1074-7613(00)80443-4 Medline

31. V. M. Salvati, T. T. MacDonald, G. del Vecchio Blanco, G. Mazzarella, I. Monteleone, P. Vavassori, S. Auricchio, F. Pallone, R. Troncone, G. Monteleone, Enhanced expression of interferon regulatory factor-1 in the mucosa of children with celiac disease. *Pediatr. Res.* **54**, 312–318 (2003). doi:10.1203/01.PDR.0000079184.70237.9C Medline

32. S. Maruyama, K. Sumita, H. Shen, M. Kanoh, X. Xu, M. Sato, M. Matsumoto, H. Shinomiya, Y. Asano, Identification of IFN regulatory factor-1 binding site in IL-12 p40 gene promoter. *J. Immunol.* **170**, 997–1001 (2003). doi:10.4049/jimmunol.170.2.997 Medline

33. L. Gabriele, A. Fragale, P. Borghi, P. Sestili, E. Stellacci, M. Venditti, G. Schiavoni, M. Sanchez, F. Belardelli, A. Battistini, IRF-1 deficiency skews the differentiation of dendritic cells toward plasmacytoid and tolerogenic features. *J. Leukoc. Biol.* **80**, 1500–1511 (2006). doi:10.1189/jlb.0406246 Medline

34. A. Fragale, L. Gabriele, E. Stellacci, P. Borghi, E. Perrotti, R. Ilari, A. Lanciotti, A. L. Remoli, M. Venditti, F. Belardelli, A. Battistini, IFN regulatory factor-1 negatively regulates $CD4^+$ $CD25^+$ regulatory T cell differentiation by repressing Foxp3 expression. *J. Immunol.* **181**, 1673–1682 (2008). doi:10.4049/jimmunol.181.3.1673 Medline

35. Y. Tada, A. Ho, T. Matsuyama, T. W. Mak, Reduced incidence and severity of antigen-induced autoimmune diseases in mice lacking interferon regulatory factor-1. *J. Exp. Med.* **185**, 231–238 (1997). doi:10.1084/jem.185.2.231 Medline

36. L. B. Ivashkiv, L. T. Donlin, Regulation of type I interferon responses. *Nat. Rev. Immunol.* **14**, 36–49 (2014). doi:10.1038/nri3581 Medline

37. H. W. Virgin, The virome in mammalian physiology and disease. *Cell* **157**, 142–150 (2014). doi:10.1016/j.cell.2014.02.032 Medline

38. K. Cadwell, K. K. Patel, N. S. Maloney, T.-C. Liu, A. C. Y. Ng, C. E. Storer, R. D. Head, R. Xavier, T. S. Stappenbeck, H. W. Virgin, Virus-plus-susceptibility gene interaction determines Crohn's disease gene Atg16L1 phenotypes in intestine. *Cell* **141**, 1135–1145 (2010). doi:10.1016/j.cell.2010.05.009 Medline

39. E. Lionetti, S. Castellaneta, A. Pulvirenti, E. Tonutti, R. Francavilla, A. Fasano, C. Catassi, Italian Working Group of Weaning and Celiac Disease Risk, Prevalence and natural history of potential celiac disease in at-family-risk infants prospectively investigated from birth. *J. Pediatr.* **161**, 908–914 (2012). doi:10.1016/j.jpeds.2012.05.008 Medline

40. R. Auricchio, A. Tosco, E. Piccolo, M. Galatola, V. Izzo, M. Maglio, F. Paparo, R. Troncone, L. Greco, Potential celiac children: 9-year follow-up on a gluten-containing diet. *Am. J. Gastroenterol.* **109**, 913–921 (2014). doi:10.1038/ajg.2014.77 Medline

41. S. Simell, S. Hoppu, A. Hekkala, T. Simell, M.-R. Ståhlberg, M. Viander, H. Yrjänäinen, J. Grönlund, P. Markula, V. Simell, M. Knip, J. Ilonen, H. Hyöty, O. Simell, Fate of five celiac disease-associated antibodies during normal diet in genetically at-risk children observed from birth in a natural history study. *Am. J. Gastroenterol.* **102**, 2026–2035 (2007). doi:10.1111/j.1572-0241.2007.01360.x Medline

42. M. Setty, V. Discepolo, V. Abadie, S. Kamhawi, T. Mayassi, A. Kent, C. Ciszewski, M. Maglio, E. Kistner, G. Bhagat, C. Semrad, S. S. Kupfer, P. H. Green, S. Guandalini, R. Troncone, J. A. Murray, J. R. Turner, B. Jabri, Distinct and synergistic contributions of epithelial stress and adaptive immunity to functions of intraepithelial killer cells and active celiac disease. *Gastroenterology* **149**, 681–691.e10 (2015). doi:10.1053/j.gastro.2015.05.013 Medline

43. M. Mäki, K. Mustalahti, J. Kokkonen, P. Kulmala, M. Haapalahti, T. Karttunen, J. Ilonen, K. Laurila, I. Dahlbom, T. Hansson, P. Höpfl, M. Knip, Prevalence of celiac disease among children in Finland. *N. Engl. J. Med.* **348**, 2517–2524 (2003). doi:10.1056/NEJMoa021687 Medline

44. B. Jabri, V. Abadie, IL-15 functions as a danger signal to regulate tissue-resident T cells and tissue destruction. *Nat. Rev. Immunol.* **15**, 771–783 (2015). doi:10.1038/nri3919 Medline

45. A. Caminero, H. J. Galipeau, J. L. McCarville, C. W. Johnston, S. P. Bernier, A. K. Russell, J. Jury, A. R. Herran, J. Casqueiro, J. A. Tye-Din, M. G. Surette, N. A. Magarvey, D. Schuppan, E. F. Verdu, Duodenal bacteria from patients with celiac disease and healthy subjects distinctly affect gluten breakdown and immunogenicity. *Gastroenterology* **151**, 670–683 (2016). doi:10.1053/j.gastro.2016.06.041 Medline

46. V. D'Argenio, G. Casaburi, V. Precone, C. Pagliuca, R. Colicchio, D. Sarnataro, V. Discepolo, S. M. Kim, I. Russo, G. Del Vecchio Blanco, D. S. Horner, M. Chiara, G. Pesole, P. Salvatore, G. Monteleone, C. Ciacci, G. J. Caporaso, B. Jabrì, F. Salvatore, L. Sacchetti, Metagenomics reveals dysbiosis and a potentially pathogenic n. flavescens strain in duodenum of adult celiac patients. *Am. J. Gastroenterol.* **111**, 879–890 (2016). doi:10.1038/ajg.2016.95 Medline

47. V. De Laurenzi, G. Melino, Gene disruption of tissue transglutaminase. *Mol. Cell. Biol.* **21**, 148–155 (2001). doi:10.1128/MCB.21.1.148-155.2001 Medline

48. M. Arnold, J. T. Patton, S. M. McDonald, Culturing, storage, and quantification of rotaviruses. *Curr. Protoc. Microbiol.*, chap. 15, unit 15C.3 (2009).

49. T. Kobayashi, A. A. R. Antar, K. W. Boehme, P. Danthi, E. A. Eby, K. M. Guglielmi, G. H. Holm, E. M. Johnson, M. S. Maginnis, S. Naik, W. B. Skelton, J. D. Wetzel, G. J. Wilson, J. D. Chappell, T. S. Dermody, A plasmid-based reverse genetics system for animal double-stranded RNA viruses. *Cell Host Microbe* **1**, 147–157 (2007). doi:10.1016/j.chom.2007.03.003 Medline

50. T. Kobayashi, L. S. Ooms, M. Ikizler, J. D. Chappell, T. S. Dermody, An improved reverse genetics system for mammalian orthoreoviruses. *Virology* **398**, 194–200 (2010). doi:10.1016/j.virol.2009.11.037 Medline

51. H. W. Virgin 4th, R. Bassel-Duby, B. N. Fields, K. L. Tyler, Antibody protects against lethal infection with the neurally spreading reovirus type 3 (Dearing). *J. Virol.* **62**, 4594–4604 (1988). Medline

52. D. B. Furlong, M. L. Nibert, B. N. Fields, Sigma 1 protein of mammalian reoviruses extends from the surfaces of viral particles. *J. Virol.* **62**, 246–256 (1988). Medline

53. R. E. Smith, H. J. Zweerink, W. K. Joklik, Polypeptide components of virions, top component and cores of reovirus type 3. *Virology* **39**, 791–810 (1969). doi:10.1016/0042-6822(69)90017-8 Medline

54. D. H. Rubin, M. J. Kornstein, A. O. Anderson, Reovirus serotype 1 intestinal infection: A novel replicative cycle with ileal disease. *J. Virol.* **53**, 391–398 (1985). Medline

55. J. D. Wetzel, J. D. Chappell, A. B. Fogo, T. S. Dermody, Efficiency of viral entry determines the capacity of murine erythroleukemia cells to support persistent infections by mammalian reoviruses. *J. Virol.* **71**, 299–306 (1997). Medline

56. E. S. Barton, J. L. Connolly, J. C. Forrest, J. D. Chappell, T. S. Dermody, Utilization of sialic acid as a coreceptor enhances reovirus attachment by multistep adhesion strengthening. *J. Biol. Chem.* **276**, 2200–2211 (2001). doi:10.1074/jbc.M004680200 Medline

57. F. Broere, M. F. du Pré, L. A. van Berkel, J. Garssen, C. B. Schmidt-Weber, B. N. Lambrecht, R. W. Hendriks, E. E. S. Nieuwenhuis, G. Kraal, J. N. Samsom, Cyclooxygenase-2 in mucosal DC mediates induction of regulatory T cells in the intestine through suppression of IL-4. *Mucosal Immunol.* **2**, 254–264 (2009). doi:10.1038/mi.2009.2 Medline

58. T. R. DiRaimondo, C. Klöck, R. Warburton, Z. Herrera, K. Penumatsa, D. Toksoz, N. Hill, C. Khosla, B. Fanburg, Elevated transglutaminase 2 activity is associated with hypoxia-induced experimental pulmonary hypertension in mice. *ACS Chem. Biol.* **9**, 266–275 (2014). doi:10.1021/cb4006408 Medline

59. B. Meresse, Z. Chen, C. Ciszewski, M. Tretiakova, G. Bhagat, T. N. Krausz, D. H. Raulet, L. L. Lanier, V. Groh, T. Spies, E. C. Ebert, P. H. Green, B. Jabri, Coordinated induction by IL15 of a TCR-independent NKG2D signaling pathway converts CTL into lymphokine-activated killer cells in celiac disease. *Immunity* **21**, 357–366 (2004). doi:10.1016/j.immuni.2004.06.020 Medline

60. G. K. Smyth, Linear models and empirical bayes methods for assessing differential expression in microarray experiments. *Stat. Appl. Genet. Mol. Biol.* **3**, e3 (2004). doi:10.2202/1544-6115.1027 Medline

61. Y. Benjamini, Y. Hochberg, Controlling the false discovery rate—A practical and powerful approach to multiple testing. *J. R. Stat. Soc. B Met.* **57**, 289–300 (1995).

62. R. Sedgewick, K. D. Wayne, *Algorithms* (Addison-Wesley, ed. 4, 2011).

63. D. Kim, G. Pertea, C. Trapnell, H. Pimentel, R. Kelley, S. L. Salzberg, TopHat2: Accurate alignment of transcriptomes in the presence of insertions, deletions and gene fusions. *Genome Biol.* **14**, R36 (2013). doi:10.1186/gb-2013-14-4-r36 Medline

64. B. Li, C. N. Dewey, RSEM: Accurate transcript quantification from RNA-Seq data with or without a reference genome. *BMC Bioinformatics* **12**, 323 (2011). doi:10.1186/1471-2105-12-323 Medline

65. D. J. McCarthy, Y. Chen, G. K. Smyth, Differential expression analysis of multifactor RNA-Seq experiments with respect to biological variation. *Nucleic Acids Res.* **40**, 4288–4297 (2012). doi:10.1093/nar/gks042 Medline

66. S. P. Smeekens, A. Ng, V. Kumar, M. D. Johnson, T. S. Plantinga, C. van Diemen, P. Arts, E. T. P. Verwiel, M. S. Gresnigt, K. Fransen, S. van Sommeren, M. Oosting, S.-C. Cheng, L. A. B. Joosten, A. Hoischen, B.-J. Kullberg, W. K. Scott, J. R. Perfect, J. W. M. van der Meer, C. Wijmenga, M. G. Netea, R. J. Xavier, Functional genomics identifies type I interferon pathway as central for host defense against *Candida albicans*. *Nat. Commun.* **4**, 1342 (2013). doi:10.1038/ncomms2343 Medline

67. J. Hitomi, D. E. Christofferson, A. Ng, J. Yao, A. Degterev, R. J. Xavier, J. Yuan, Identification of a molecular signaling network that regulates a cellular necrotic cell death pathway. *Cell* **135**, 1311–1323 (2008). doi:10.1016/j.cell.2008.10.044 Medline

68. R. DeJesus, F. Moretti, G. McAllister, Z. Wang, P. Bergman, S. Liu, E. Frias, J. Alford, J. S. Reece-Hoyes, A. Lindeman, J. Kelliher, C. Russ, J. Knehr, W. Carbone, M. Beibel, G. Roma, A. Ng, J. A. Tallarico, J. A. Porter, R. J. Xavier, C. Mickanin, L. O. Murphy, G. R. Hoffman, B. Nyfeler, Functional CRISPR screening identifies the ufmylation pathway as a regulator of SQSTM1/p62. *eLife* **5**, e17290 (2016). doi:10.7554/eLife.17290 Medline

69. P. W. Lord, R. D. Stevens, A. Brass, C. A. Goble, Investigating semantic similarity measures across the Gene Ontology: The relationship between sequence and annotation. *Bioinformatics* **19**, 1275–1283 (2003). doi:10.1093/bioinformatics/btg153 Medline

70. A. Schlicker, F. S. Domingues, J. Rahnenführer, T. Lengauer, A new measure for functional similarity of gene products based on Gene Ontology. *BMC Bioinformatics* **7**, 302 (2006). doi:10.1186/1471-2105-7-302 Medline